KNOW-BLADE task-3.2 report: Tip shape study

Sørensen, Niels N.; Johansen, Jeppe; Conway, S.; Voutsinas, S.; Hansen, M.O.L.; Stuermer, A.

Publication date:
2005

Document Version
Publisher's PDF, also known as Version of record

Risø-R-1495(rev)(EN)

KNOW-BLADE
Task-3.2 report
Tip Shape Study
revised version

N. N. Sørensen, J. Johansen, S. Conway,
S. Voutsinas, M.O.L. Hansen, A. Stürmer

Risø National Laboratory, Roskilde, Denmark
January 2005

1 Abstract

For modern rotor blades with their very large aspect ratio, the blade tip is a very limited part of the overall rotor, and as such of limited importance for the overall aerodynamics of the rotor. Even though they may not be very important for the overall power production, the tip noise can be very important for the acoustics of the rotor [15], and the blade tips can as well be important for the aerodynamic damping properties of the rotor blades [13]. Unfortunately, not many options exists for predicting the aerodynamic behavior of blade tips using computational methods. Experimentally it is difficult to perform detailed measurements in the form of pressure and velocity measurements in natural wind conditions on modern large scale turbines due to the inherent unsteadiness in the natural wind.

The present study describes the application of four different Navier-Stokes solvers to tip shape studies, and shows that these codes are well suited to study the flow around different tip shape geometries, and can predict the pressure distributions at the blade tip quite accurately.

Contents

1 Abstract *2*

2 Introduction *5*

3 Methods *6*
3.1 Navier-Stokes Solvers *6*

4 Geometrys and computational meshes *8*
4.1 Surface generation *8*
4.2 Volume Mesh Generation *8*
4.3 Boundary Conditions *8*

5 Results, STORK 5.0 WPX *11*

6 Conclusion: STORK 5.0 WPX *17*

7 Results LM8.2 *26*

8 Conclusion LM8.2 blades *28*

9 Conclusion *45*

10 Acknowledgement *45*

2 Introduction

The present work is made during the KNOW-BLADE EC project (contract number: ENK6-CT-2001-00503) in which nine partners are involved. These are:

Risø National Laboratory, Roskilde Denmark,	RISOE (Coordinator)
Centre for Renewable Energy Sources, Greece,	CRES
Deutches Zentrum fuer Luft- und Raumfahrt, Germany	DLR
Danmarks Tekniske Universitet, Denmark	DTU
Swedish Defence Research Agency, Sweden,	FOI
National Technical University of Athens, Greece	NTUA
Vrije Universiteit Brussels, Belgium	VUB
Foundation of Research and Technology, Greece	FORTH
LM Glasfiber A/S, Denmark	LMG

The main objective of the project is through research activities to fill in important knowledge gaps in the wind turbine community by applying Navier-Stokes (NS) solvers to a series of unsolved aerodynamic and aeroelastic problems. The present report describes the work carried out in work package WP3: Tip shape studies in which DLR, DTU, FOI, RISOE, VUB are involved.

For modern rotor blades with their very large aspect ratio, the blade tip is a very limited part of the overall rotor, and as such of limited importance for the overall aerodynamics of the rotor. Even though they may not be very important for the power production, tip noise can be very important for the acoustics of the rotor [15], and the blade tips can as well be important for the aerodynamic damping properties of the rotor blades [13]. Unfortunately, not many options exist for predicting the aerodynamic behaviour of blade tips. Standard Blade Element Momentum methods and lifting line models used in wind turbine industry do not offer much information about the aerodynamics of the blade tips. Experimentally, it is difficult to perform detailed measurements in the form of pressure and velocity measurements in natural wind conditions on modern large scale turbines due to the inherent unsteadiness in the natural wind, the few measurements that exist lack detailed flow information [7]. For modern turbines, wind tunnel measurements are not an option, and the data that exists are all for smaller turbines [3, 16, 5]. One possible option to study different tip shapes is the application of Navier-Stokes solvers, and in the present study a series of Computational Fluid Dynamics (CFD) Navier-Stokes solvers are applied to the this problem. First a validation study is carried out on turbine with STORK 5.0 WPX blades, where measurements exist from a wind tunnel. Following this validation study, a parametric study of four tips corresponding to an existing experiment on a Tellus turbine equipped with LM8.2 blades with different tip shapes is carried out.

3 Methods

In the present work a series of different Navier-Stokes solvers both compressible and incompressible are applied to rotor computations with specific focus on the flow around the blade tips. Below a short description is given of the individual solvers and how they were used for the present applications. Originally it was planned to investigate the possibility of performing rotating and non-rotating computations respectively. As the non-rotating results proved to be unsuited to evaluate the tips during rotations, these results will not be discussed further in this report.

3.1 Navier-Stokes Solvers

The Risø/DTU EllipSys3D code is developed in co-operation between the Department of Mechanical Engineering at DTU and The Department of Wind Energy at Risø National Laboratory, see Michelsen[10, 11] and Sørensen[18]. The EllipSys3D code is a multiblock finite volume discretization of the incompressible Reynolds Averaged Navier-Stokes (RANS) equations in general curvilinear coordinates. As the code solves the incompressible flow equations, no equation of state exists for the pressure, and the PISO algorithm of Issa [8], [9] is used to enforce the pressure/velocity coupling. The solution of the Poisson system arising from the pressure correction equation is accelerated using a multigrid method. The solution is advanced in time using a 2nd order iterative time-stepping (or dual time-stepping) method. In each global time-step the equations are solved in an iterative manner, using underrelaxation. The convective terms are discretized using a third order upwind scheme, implemented using the deferred correction approach first suggested by Khosla and Rubine [14]. Central differences are used for the viscous terms. In each sub-iteration only the normal terms are treated fully implicit, while the terms from non-orthogonality and the variable viscosity terms are treated explicitly. For the present application a non-inertial reference frame attached to the rotor blades is used, and extra terms accounting for the Coriolis and centripetal forces are added to the equations. Polar velocities are used to allow simple treatment of periodic boundary conditions in the azimuthal direction[19, 12]. The turbulence in the boundary layer is modeled by the k-ω SST eddy viscosity model of Menter [21]. The EllipSys3D code is parallelized with MPI for execution on distributed memory machines, using a non-overlapping domain decomposition technique.

The NTUA code is solving the steady RANS equations within the Finite Volume Method context. The core of the computation considers a C-type grid that surrounds the blade. Then there is the option to either embed this grid to a cylindrical grid extending both upwind and downstream representing the RANS-RANS option, or couple the RANS solver with a free-wake vortex particle flow solver representing the RANS-VORTEX option. The coupling of the separate blocks in the RANS-RANS option is done using the chimera strategy. The coupling of the two methods in the RANS-VORTEX method is done by matching the velocity at the boundary of the RANS domain. The RANS-RANS option is more expensive compared to the RANS-VORTEX which is suitable for systematic runs. Otherwise, the RANS solver is using staggered topology and the SIMPLE algorithm for determining the pressure field. As regards turbulence closure, there are two options: the $k-\omega$ SST and the Spalart-Allmaras eddy viscosity models.

The FOI EDGE solver, is a flow solver for unstructured grids of arbitrary elements, see [20]. EDGE solves the Reynolds Averaged Navier-Stokes compressible equations in either a steady frame of reference or in a frame with system rotation.

Turbulence can be modelled with differential eddy viscosity models or explicit algebraic Reynolds stress models. The solver is based on an edge-based formulation and uses a node-centered finite-volume technique to solve the governing equations. The control volumes are non-overlapping and are formed by a dual grid obtained from the control surfaces for each edge. All elements are connected through matching faces. The governing equations are integrated explicitly towards steady state with Runge- Kutta time integration. The convergence is accelerated with agglomeration multigrid and implicit residual smoothing. EDGE contains different spatial discretizations for the mean flow as well as the turbulence, different gas models, steady state and time accurate time integration, low speed preconditioning etc. The turbulence in the boundary layer is modeled by the original k-ω eddy viscosity model of Wilcox [4], and the Wallin and Johansson explicit Algebraic Stress Model based on the Wilcox k-ω model [25]. For the present computations the central difference scheme with artificial dissipation is used for the convective terms.

The DLR TAU-code, developed in the MEGAFLOW project[17], is a 3D unstructured finite-volume CFD software package for the numerical simulation of a wide range of aerodynamic flows using the compressible Euler or Reynolds-averaged Navier-Stokes equations. It utilizes an edge based data structure, also referred to as a dual grid approach, which serves to improve the memory efficiency of the solver and allows arbitrarily shaped mesh elements to be used. Various schemes are available for the discretization of the convective terms, including Roe- or AUSM-type second order upwind schemes as well as central differencing schemes coupled with scalar or matrix dissipation. The viscous fluxes are discretized with a central scheme. For steady state computations an explicit multi-stage Runge-Kutta scheme is employed for the temporal integration of the governing equations, while for time-accurate computations the dual time-stepping approach is used. Acceleration of convergence is accomplished using residual smoothing, local time-stepping and multigrid techniques. Among the turbulence models implemented in TAU are the one-equation Spalart-Allmaras [22] and the two-equation Menter-SST model. The simulation of multi-body geometries in relative motion is made possible in the TAU-code through the Chimera grid technique [2, 1]. Furthermore, the DLR-TAU code offers solution based grid adaptation both through addition as well as the redistribution of grid nodes as required to improve resolution of important aerodynamic flow features. For the tip shape studies presented here the TAU code was run using a central discretization of the convective fluxes with scalar dissipation, a 3V-multigrid cycle and the Spalart-Allmaras turbulence model. A steady-state computation was possible due to the flow being steady in the grid frame which rotates along with the blade.

4 Geometrys and computational meshes

For the computations described in the present report, a common mesh was constructed for each case by RISOE. The NTUA code using orthogonal meshes could not use these common meshes and NTUA constructed meshes specifically for their solver. A short description of how the meshes where generated is given below.

4.1 Surface generation

Based on the sectional information digital surface geometry descriptions were generated. The last few percent of the span, where the surface is double curved, a NURBS surface generator is used. For the main part of the blades inhouse RISOE software was used to construct surface meshes based on the digitized surfaces, while the outermost 5 % of the blade near the tip, where the surface is strongly double curved, either the MEGACADS program by DLR or an inhouse hyperbolic surface generator by RISOE was used. The surface mesh has 256 cells in the chordwise direction, 64 cells in the spanwise direction, and one extra block to resolve the blade tip.

4.2 Volume Mesh Generation

Generating the volume mesh for the different rotors, respectively the 120 and the 80 degrees periodicity of the rotor, are exploited by only meshing one blade. The remaining blades are included in the computations through the use of periodic boundary conditions. In the following the construction of the volume mesh for the 120 degrees section is described, the two bladed mesh is generate in a similar fashion. Based on the 5 block surface mesh, an O-O-mesh is constructed around the blade using the Risø HypGrid3D hyperbolic mesh generation code. The O-O-topology extends approximately one rotor radius up and downstream of the rotor disc, and span 120 degrees in the rotation direction. The cells at the wall has a $y^+ \sim 2$ to resolve the laminar sublayer, and the points are distributed in normal direction using a hyperbolic tangent function. To take the farfield boundary approximately 5 rotor diameters away from the rotor, an outer 3 block O-configuration was added on top of the inner O-O-configuration. The total mesh has around 2 million cells, see Fig. 1.

Two meshes are constructed for the computations of the two bladed STORK rotor, one used for the free computations see Fig. 2 and one used for the tunnel configuration see Fig. 3. As seen from the figure the tunnel is approximated using a cylindrical cross section with an area equal to 144 [m^2]. The inner part of the two meshes close to the rotor blades are identical, while the outer part is changed in order to model either the free or the tunnel configuration.

4.3 Boundary Conditions

The following boundary conditions are used in the computations. For the spherical 'free' meshes on the upstream part of the outer spherical part of the domain, the part of the outer boundary visible in Fig. 1 the undisturbed velocity is specified. On the downstream part of the outer boundary fully developed conditions are assumed. On the inner cylindrical boundary along the rotational axis Euler/Slip conditions are specified, while no-slip conditions are specified on the blade of the surface. Finally fully implicit periodic conditions are specified on the two 120

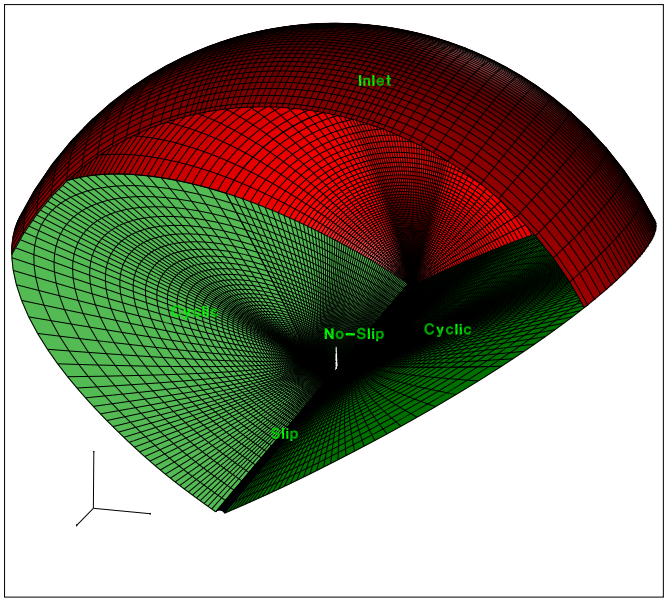

Figure 1. The spherical mesh around the LM8p2 rotor, the outer diameter of the domain is approximately 6 rotor diameters.

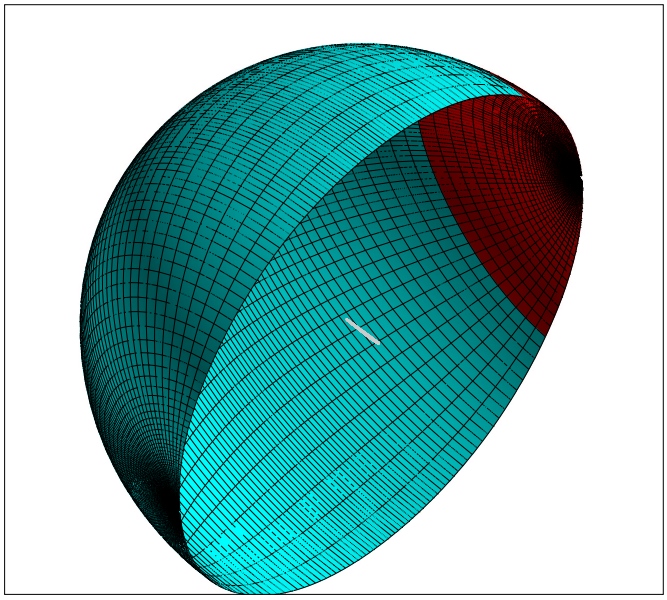

Figure 2. The spherical mesh around the free configuration for the STORK 5 WPX, the outer diameter of the domain is approximately 6 rotor diameters.

degrees periodic planes. For the cylindrical 'tunnel' mesh the undisturbed velocity is specified at the upstream lid, while fully developed conditions are assumed at the downstream lid. At the outer cylindrical face an Euler/slip conditions is used.

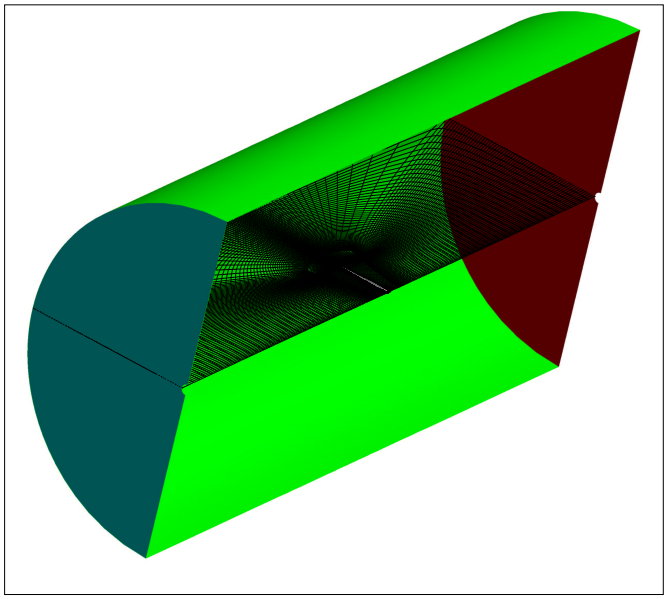

Figure 3. The cylindrical mesh around the tunnel configuration, the outer diameter of the domain is approximately 2 rotor diameters.

5 Results, STORK 5.0 WPX

To verify the applicability of modern CFD codes to study the flow around wind turbine blade tips, a series of computations of a turbine equipped with two STORK 5.0 WPX blades were performed. Static pressure distributions has been measured during a wind tunnel study of the STORK 5.35 meter rotor in the CARDC (China Aerodynamic Research and Development Centre) low speed wind tunnel [6],[23]. Especially in connection with tip studies, the fact that pressure was measured at several spanwise stations closed to the blade tip, makes the wind tunnel study well suited for the present purpose. Measurements from the study was made available to the present project by FOI, and four cases were selected corresponding to tip speed ratios in the range of 5.5 to 9, see Table 1. The density are in all cases specified to 1.225 [kg/m^3] and the viscosity is 1.78791^{-5} [kg m/s^2]. The tip pitch is set at two degrees, pitching the blade towards lower angles of attack.

CASE	Pitch [deg.]	RPM	Wind Speed [m/s]	Blockage Corrected Wind Speed [m/s]
13	2	155.36	7.66	7.84
14	2	183.76	7.67	7.89
15	2	215.10	7.65	7.92
16	2	243.57	7.64	7.94

Table 1. The run parameters for the four investigated cased.

CASE	Power [kW]			Thrust [N]		
	Measured	Free	Tunnel	Measured	Free	Tunnel
13	2.515	2.260	2.220	467.7	416.0	419.2
14	2.979	2.536	2.474	544.8	486.6	489.4
15	3.248	2.692	2.599	611.0	551.6	551.8
16	3.094	2.713	2.582	657.9	598.0	594.8

Table 2. Computed power and thrust for the free and the tunnel configuration.

First a series of computations are performed according to the run conditions reported by FFA/FOI, both for the free and the tunnel configuration. When using the tunnel measurements under free conditions, a correction for the tunnel blockage has to be applied according to Eqn. 1 as given in [24]. Comparing the computed power for the free and the tunnel configuration, as given in Table 2, a relatively good agreement between the two series of computations is seen. Based on this and the fact that a minimal difference between the pressure distributions from the tunnel and the free computations can be observed see Figurs 4 to 7, the blockage correction suggested by FFA/FOI seems to be well working.

$$\Delta V/V_{uncorrected} = 0.0379 C^2_{Tuncorrected} + .01 \quad (1)$$

From Table 2, it is seen that both the free and the tunnel computations exhibits considerable under-prediction compared to measurements. This is in contrast to

the general observation where normally very good agreement is observed at these tip speed ratios. As the deviation of both power and thrust is unusual large, an attempt was made to determine an increased velocity that would result in the correct power and thrust. A series of computations for case 13 and 16 are performed, showing that increasing the velocity around 6 percent resulted in an improvement of the agreement in both power and thrust, see Table 3. An additional indicator that the velocity may be underestimated in the experiment, is seen from the fact that also the detailed pressure distributions show improved agreement performing computations with the increased velocity, see Fig. 4 to 7.

CASE	Velocity [m/s]	Power [kW]		Thrust [N]	
	(corrected)	Measured	Computed	Measured	Computed
13	8.11	2.515	2.533	467.7	446.7
14	8.13	2.979	2.863	544.8	523.2
15	8.11	3.248	3.054	611.0	594.8
16	8.10	3.094	3.099	657.9	645.7

Table 3. Comparison of computed and measured power and thrust for CASE 13 to 16 using a 6 percent increased inflow velocity.

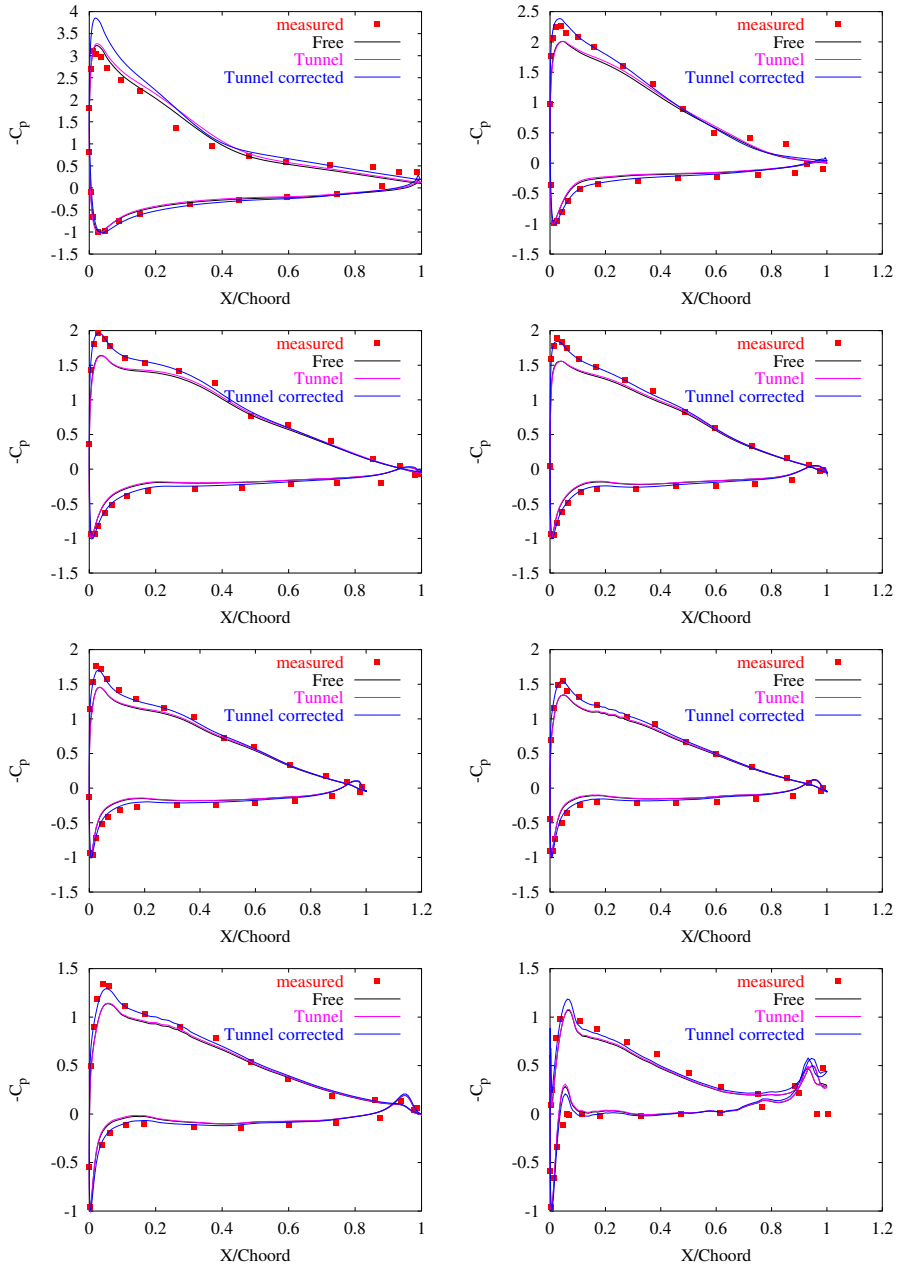

Figure 4. Comparison of computed and measured pressure for the tunnel and free configuration of CASE 13. A computation with 6 percent increased inlet velocity is included. The figure shows from top left to bottom right the spanwise sections [0.30, 0.55, 0.75, 0.85, 0.925, 0.95, 0.975, 0.99].

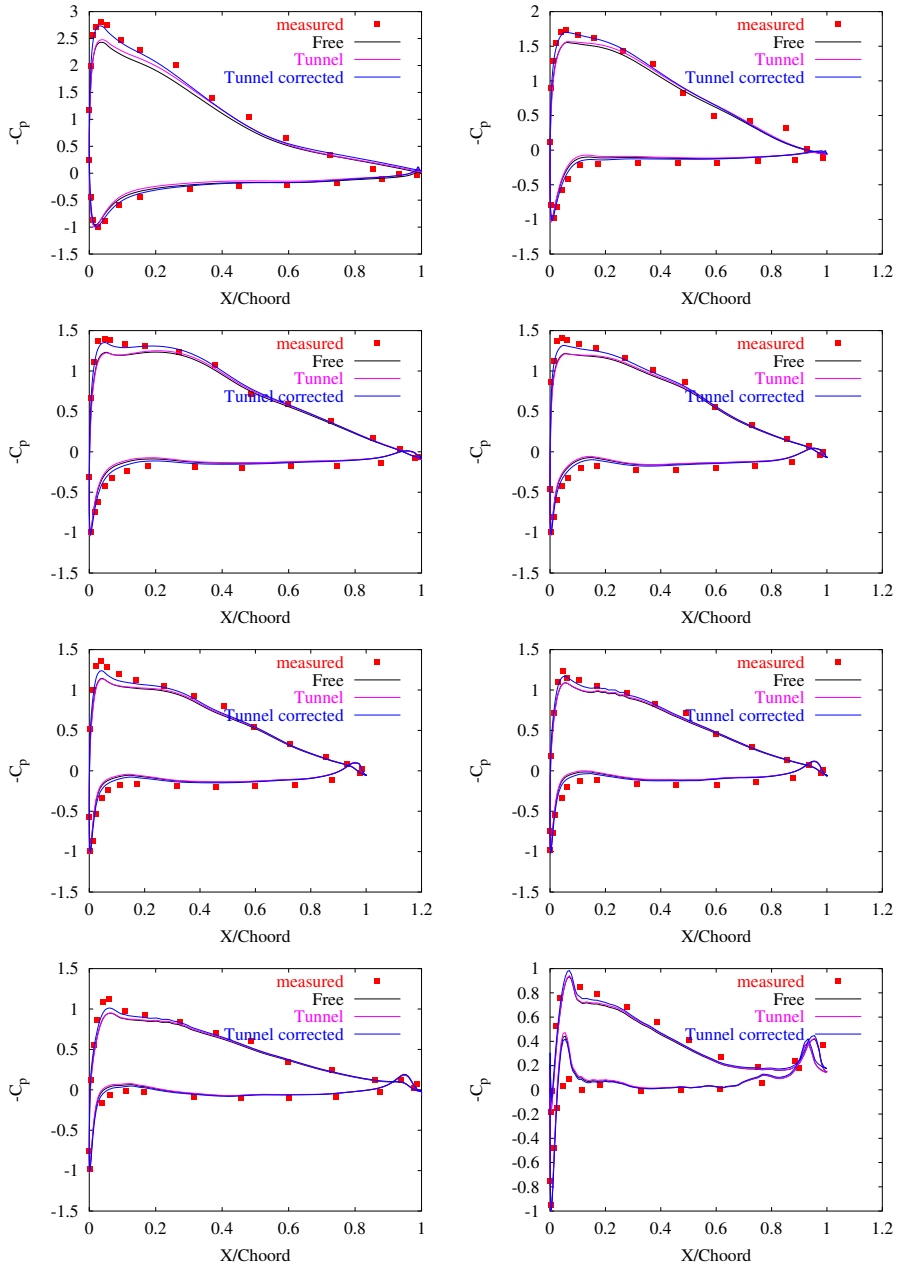

Figure 5. Comparison of computed and measured pressure for the tunnel and free configuration of CASE 14. A computation with 6 percent increased inlet velocity is included. The figure shows from top left to bottom right the spanwise sections [0.30, 0.55, 0.75, 0.85, 0.925, 0.95, 0.975, 0.99].

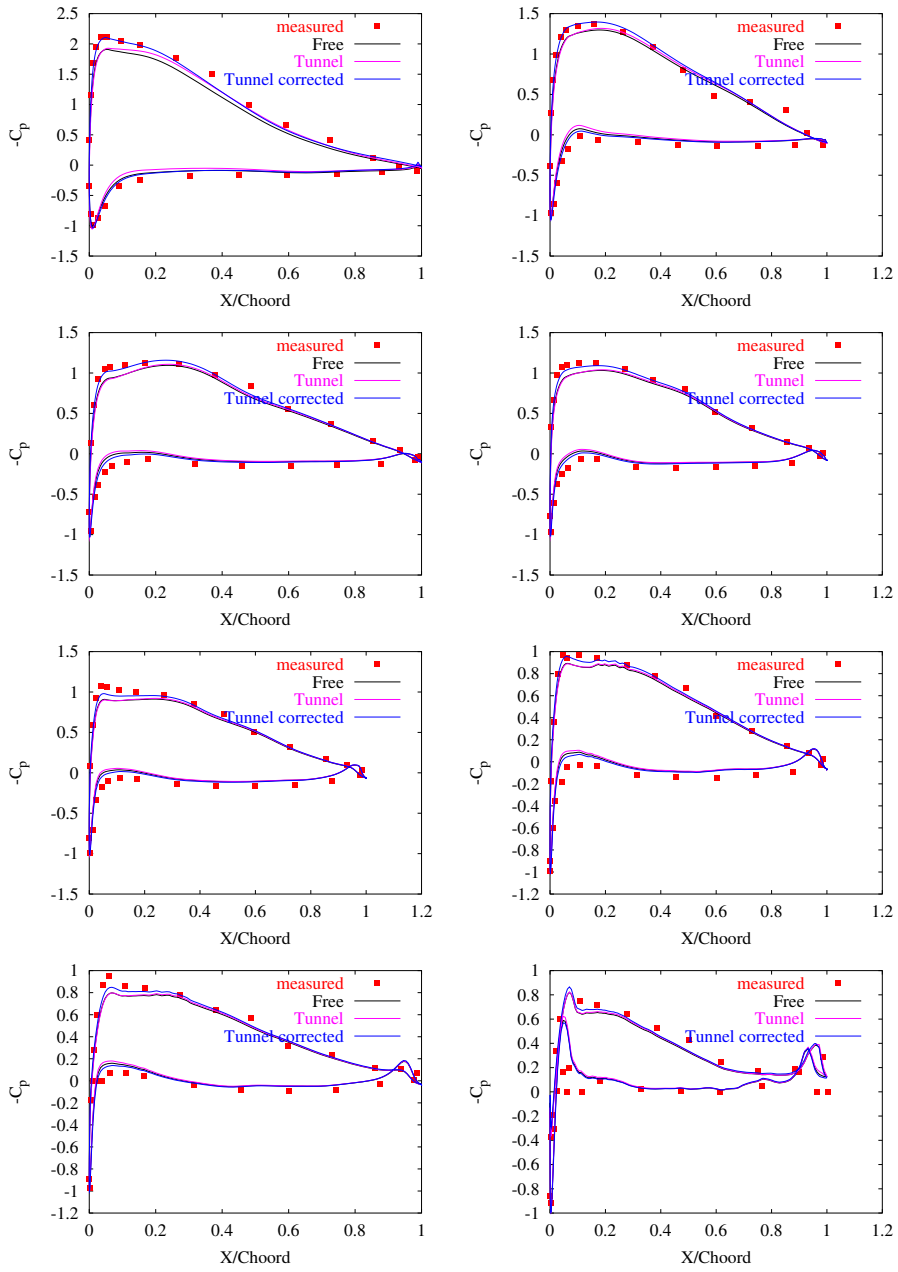

Figure 6. Comparison of computed and measured pressure for the tunnel and free configuration of CASE 15. A computation with 6 percent increased inlet velocity is included. The figure shows from top left to bottom right the spanwise sections [0.30, 0.55, 0.75, 0.85, 0.925, 0.95, 0.975, 0.99].

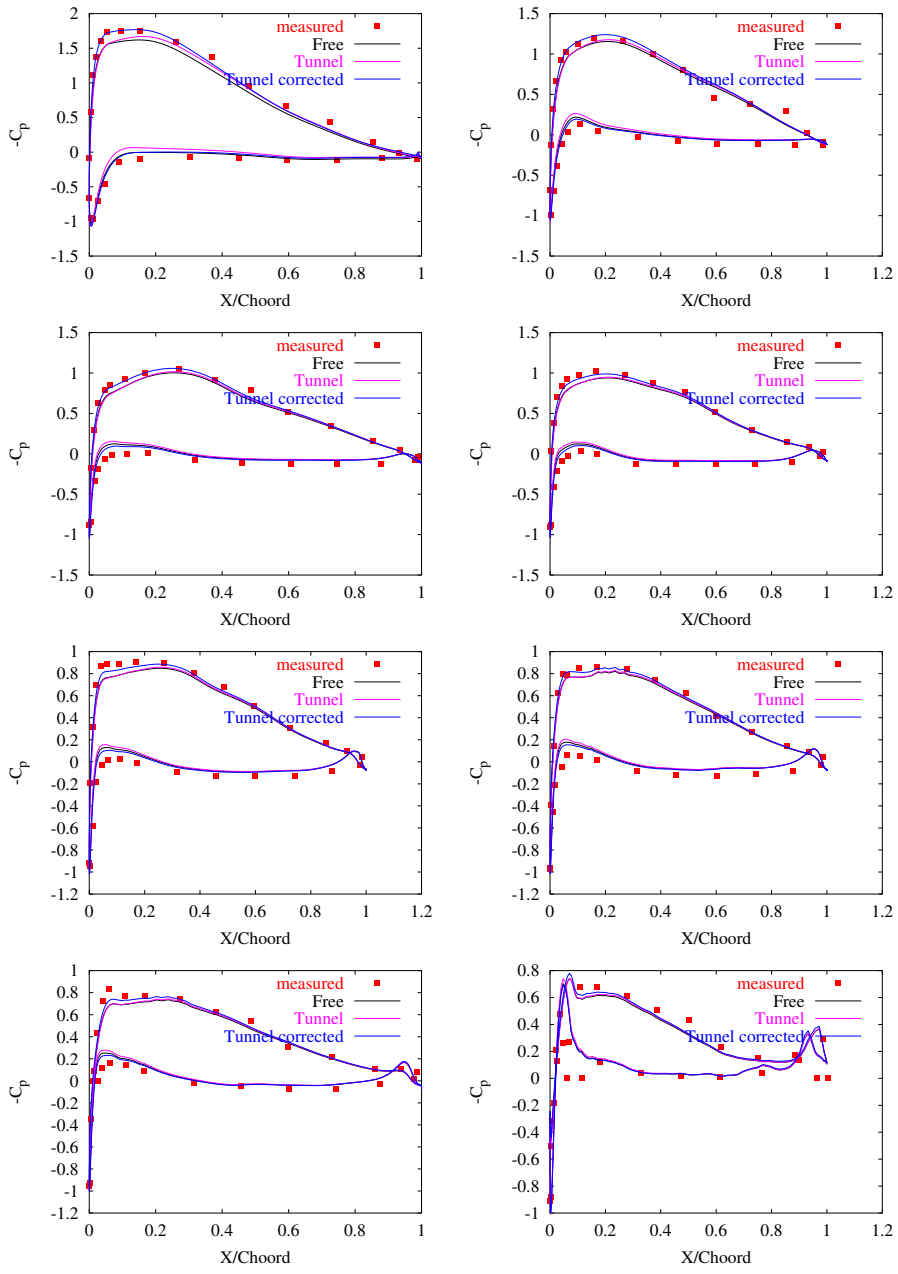

Figure 7. Comparison of computed and measured pressure for the tunnel and free configuration of CASE 16. A computation with 6 percent increased inlet velocity is included. The figure shows from top left to bottom right the spanwise sections [0.30, 0.55, 0.75, 0.85, 0.925, 0.95, 0.975, 0.99].

Having documented, that the blockage correction proposed by FFA/FOI are working well, and illustrated that there may be problems with the measured wind speed in the wind tunnel, the following part of the report will focus on a comparison of the RISOE and FOI flow solvers and their application to tip computations. Comparing the power computed by the RISOE, EllipSys3D and by the FOI, EDGE code, the prediction by the EDGE code is 8 to 19 % lower than the EllipSys3D predictions. From the spanwise force distributions on Figure 8 the low driving force (Fx) on the central part of the blade, caused by the EDGE computations predicting the separation line more towards the leading edge, is responsible for the lower power production. The reason for this difference is not clear, but as both models uses the same mesh and same turbulence model, it may be connected to the handling of extreme low speed regions by the compressible EDGE code.

Looking at the sectional pressure distributions Figure 9 to 12 the problems observed in the force distributions are clearly visible on the inboard part of the blade, where both computations underestimate the suction compared to the measurements, with a pronounced lack of suction in the FOI results. On the outboard part of the blade, an excellent agreement is observed between the two series of computations but as discussed earlier on, a weak underprediction compared to measurements is found in this area.

The limiting streamlines on the suction side of the blade for CASE 13 is shown on Fig. 14, revealing that the amount of separated flow decreases when increasing the tip speed ratio from approximately five at the top to eight at the bottom of the figure. From this figure it is clear that for all the computed cases, at least the outermost forty percent of the rotor is fully attached. This is in good agreement with what was deduced from the pressure distributions. The detailed pictures of the flow patterns at the blade tip, Figure 15, shows how the region influenced by the tip vortex diminishes as the tip speed ratio is raised form CASE 13 to CASE 16.

CASE	Power [kW]			Thrust [N]		
	Measured	RISOE	FOI	Measured	RISOE	FOI
13	2.515	2.260	1.980	467.7	416.0	-
14	2.979	2.536	2.314	544.8	486.6	-
15	3.248	2.692	2.360	611.0	551.6	-
16	3.094	2.713	2.187	657.9	598.0	-

Table 4. Comparison of measured and computed power and thrust for the four investigated configurations.

6 Conclusion: STORK 5.0 WPX

A series of computations of the STORK 5.0 WPX rotor corresponding to measured conditions from a wind tunnel experiment has been performed. Computations was first made comparing a free and a tunnel configuration, using the RISOE EllipSys3D code to verify the blockage correction suggested by FFA. The initial computations showed an underprediction of the power even at the high tip speed ratio, and further inquiries were initiated. It was found by systematic increasing the velocity in the computations, that both the power and the detailed pressure

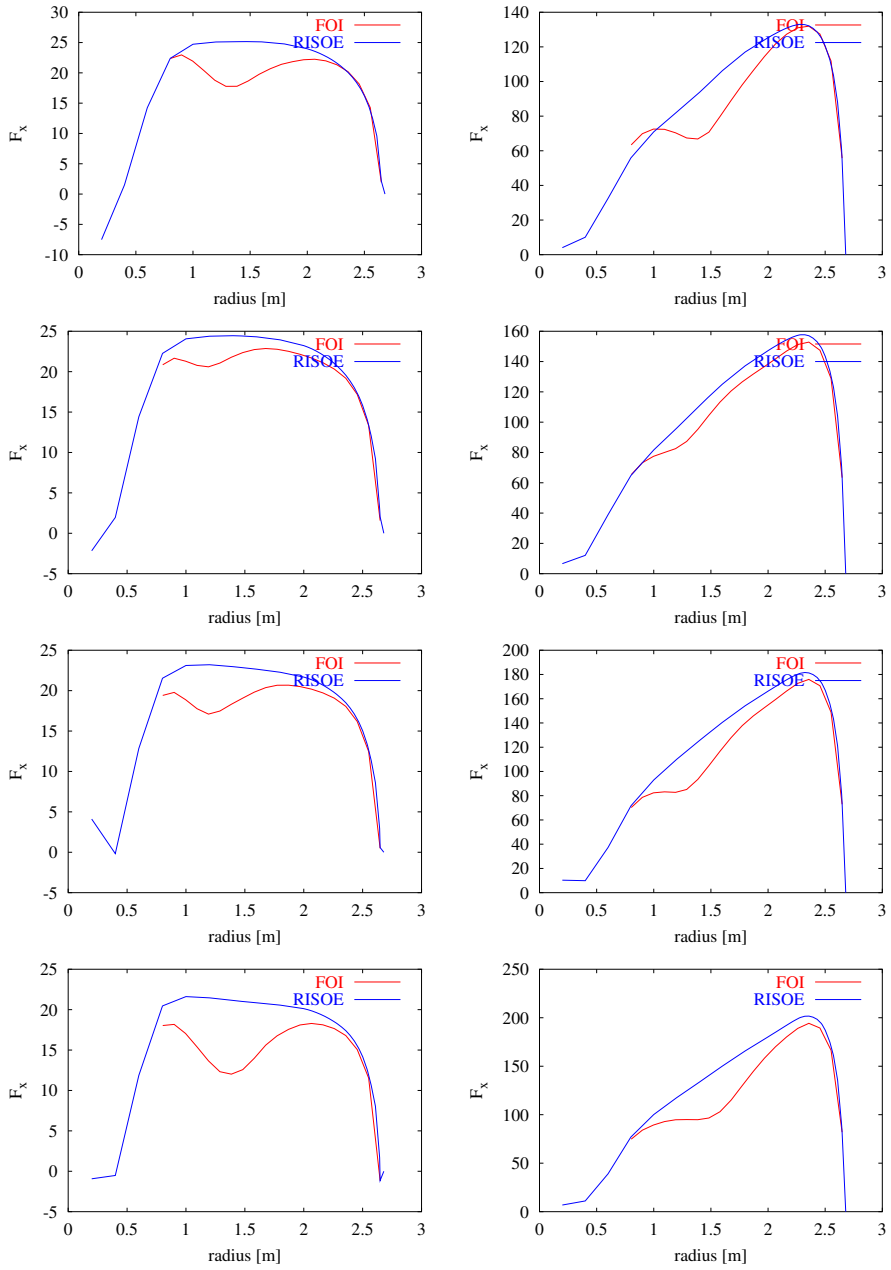

Figure 8. Comparison of the spanwise force distributions computed by FOI and RISOE. Showing from top to bottom the tangential and axial force distributions for CASE 13 to 16.

distributions showed improved agreement when increasing the tunnel speed by six percent. This investigation indicates that there may be a problem with the velocity measured in the tunnel. Finally, the FOI, EDGE solver and the RISOE, EllipSys3D solver were compared to measurements for four cases. Except for the inboard part of the rotor, were large areas of separation exists especially for low tip speed ratios, a very good agreement was found for the two Navier-Stokes solvers. This indicates that CFD solvers predict consistent results for tip shape studies. Except for the underprediction on the inboard part of the rotor, the solutions showed good agreement with measurements both qualitative and quantitative. It must be concluded that Navier-Stokes solutions can be used to evaluate tip

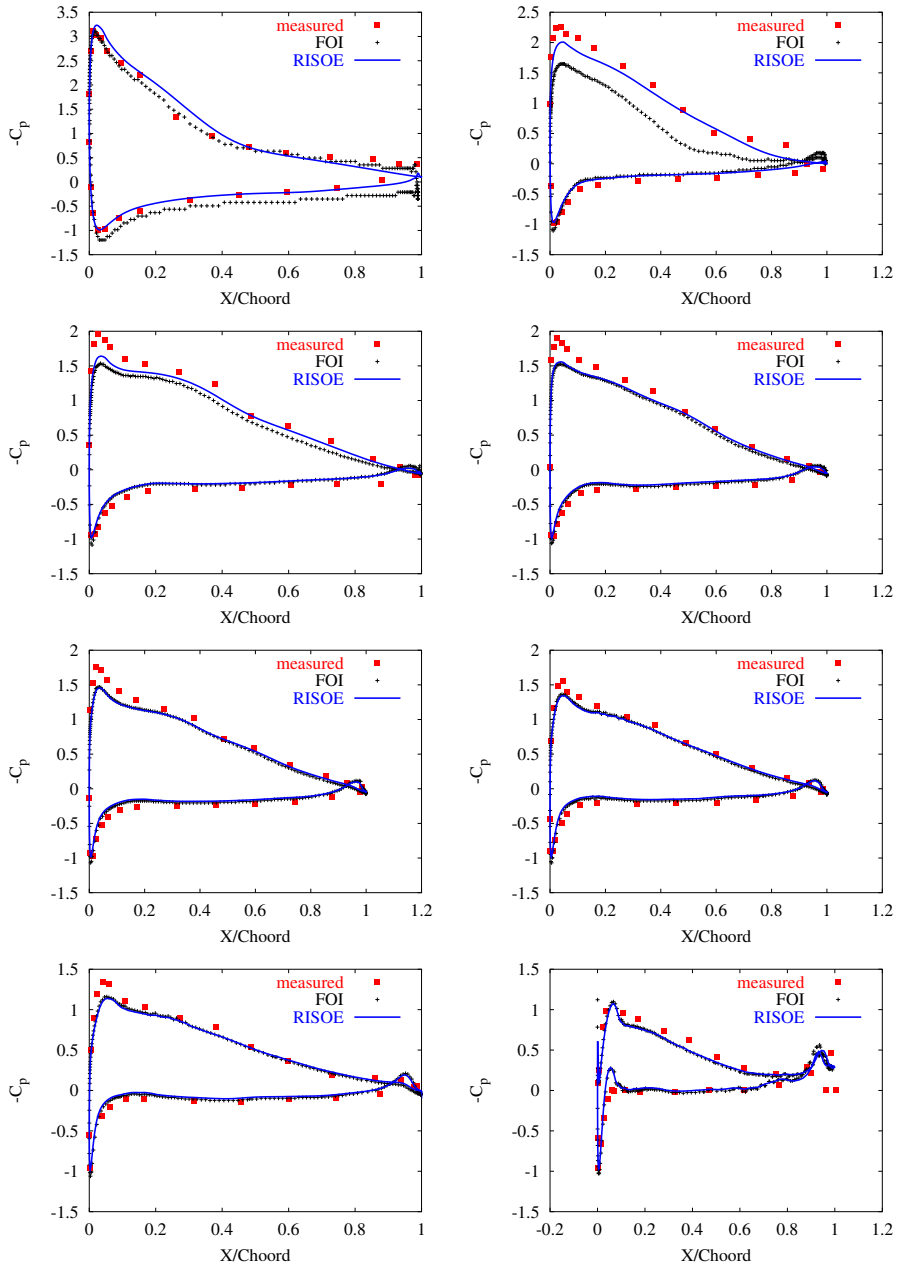

Figure 9. Comparison of computed and measured pressure for the free configuration of CASE 13 using the blockage corrected wind speed. The figure shows from top left to bottom right the spanwise sections [0.30, 0.55, 0.75, 0.85, 0.925, 0.95, 0.975, 0.99]

shapes, and that the solutions offer a very high level of details that cannot be easily obtained using other methods.

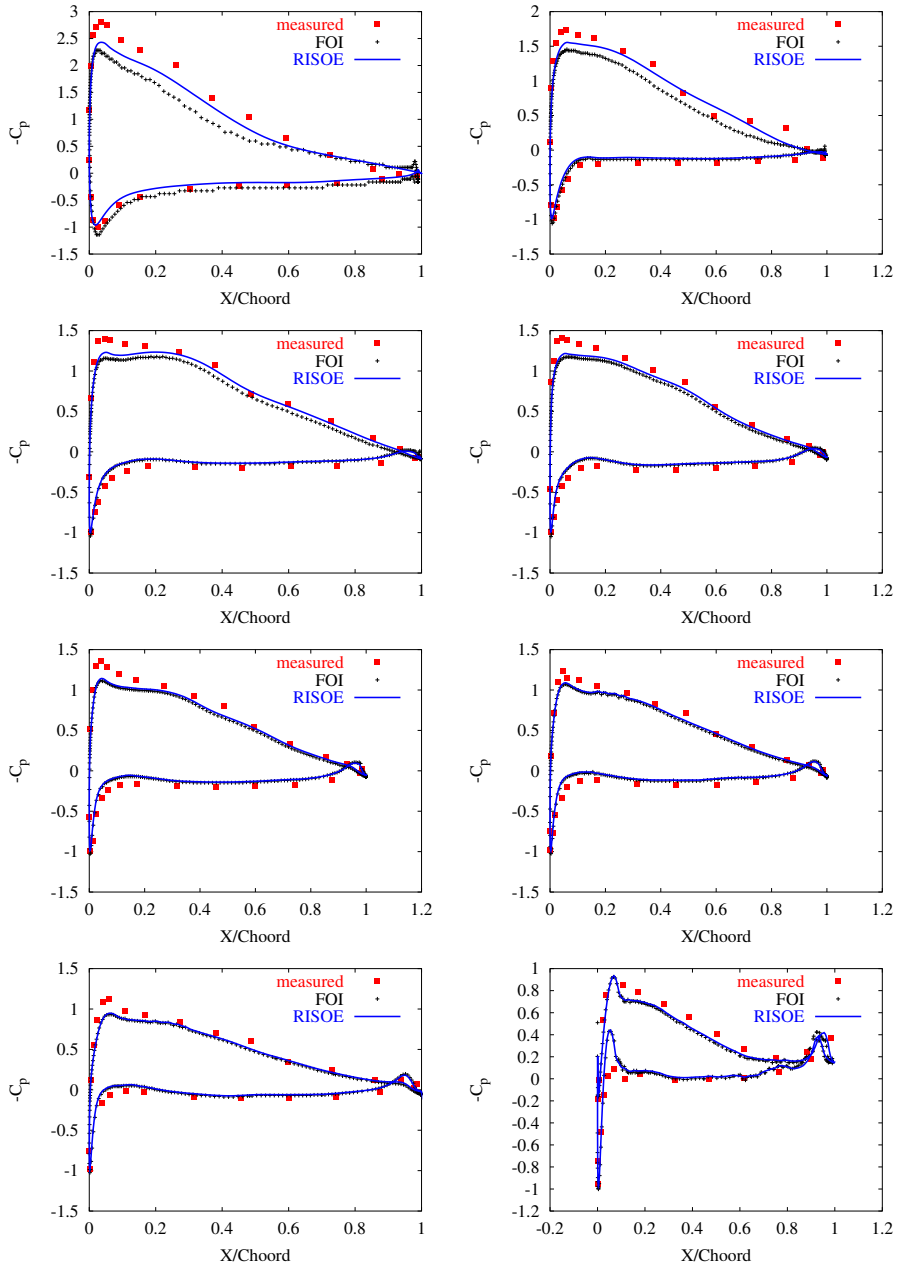

Figure 10. Comparison of computed and measured pressure for the free configuration of CASE 14 using the blockage corrected wind speed. The figure shows from top left to bottom right the spanwise sections [0.30, 0.55, 0.75, 0.85, 0.925, 0.95, 0.975, 0.99]

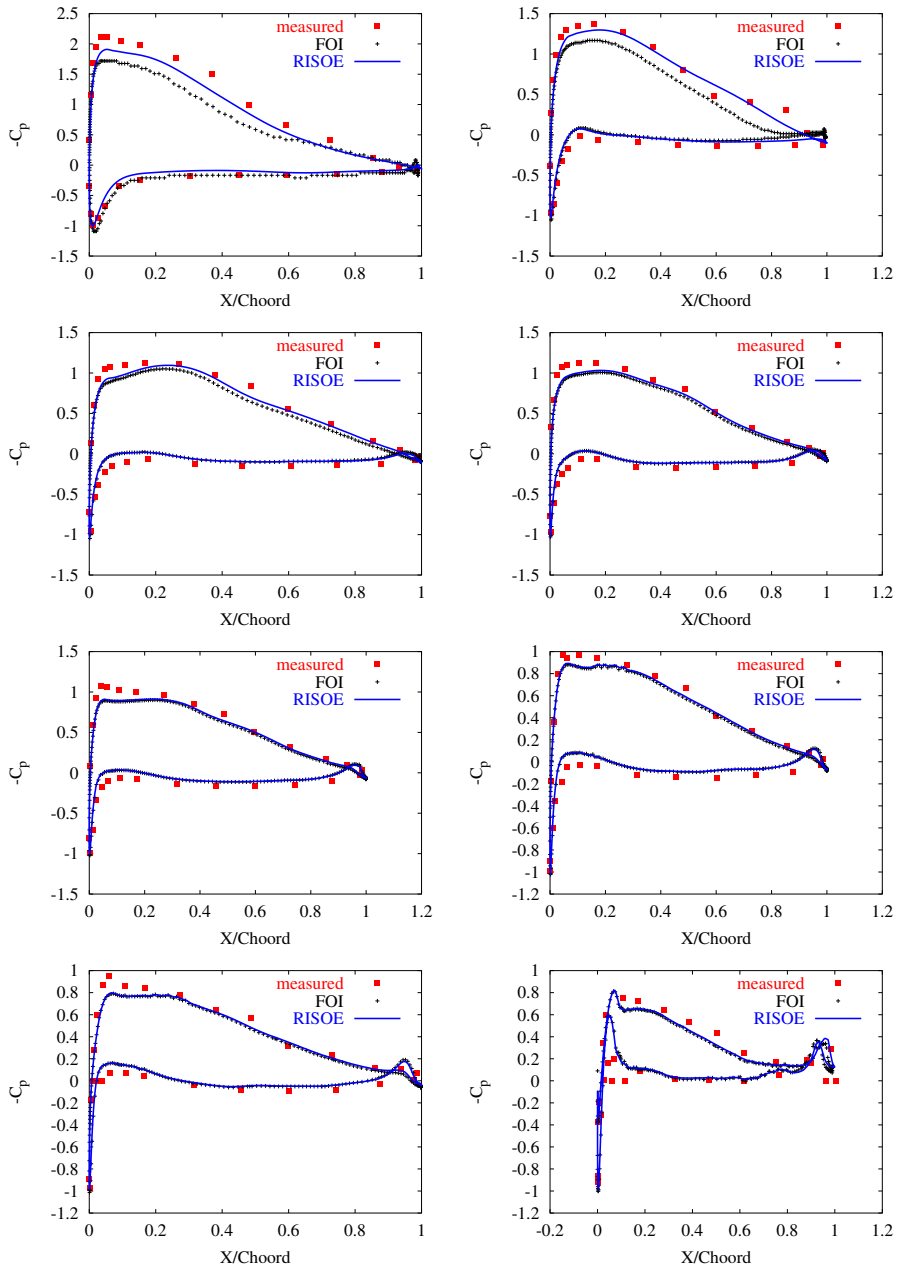

Figure 11. Comparison of computed and measured pressure for the free configuration of CASE 15 using the blockage corrected wind speed. The figure shows from top left to bottom right the spanwise sections [0.30, 0.55, 0.75, 0.85, 0.925, 0.95, 0.975, 0.99]

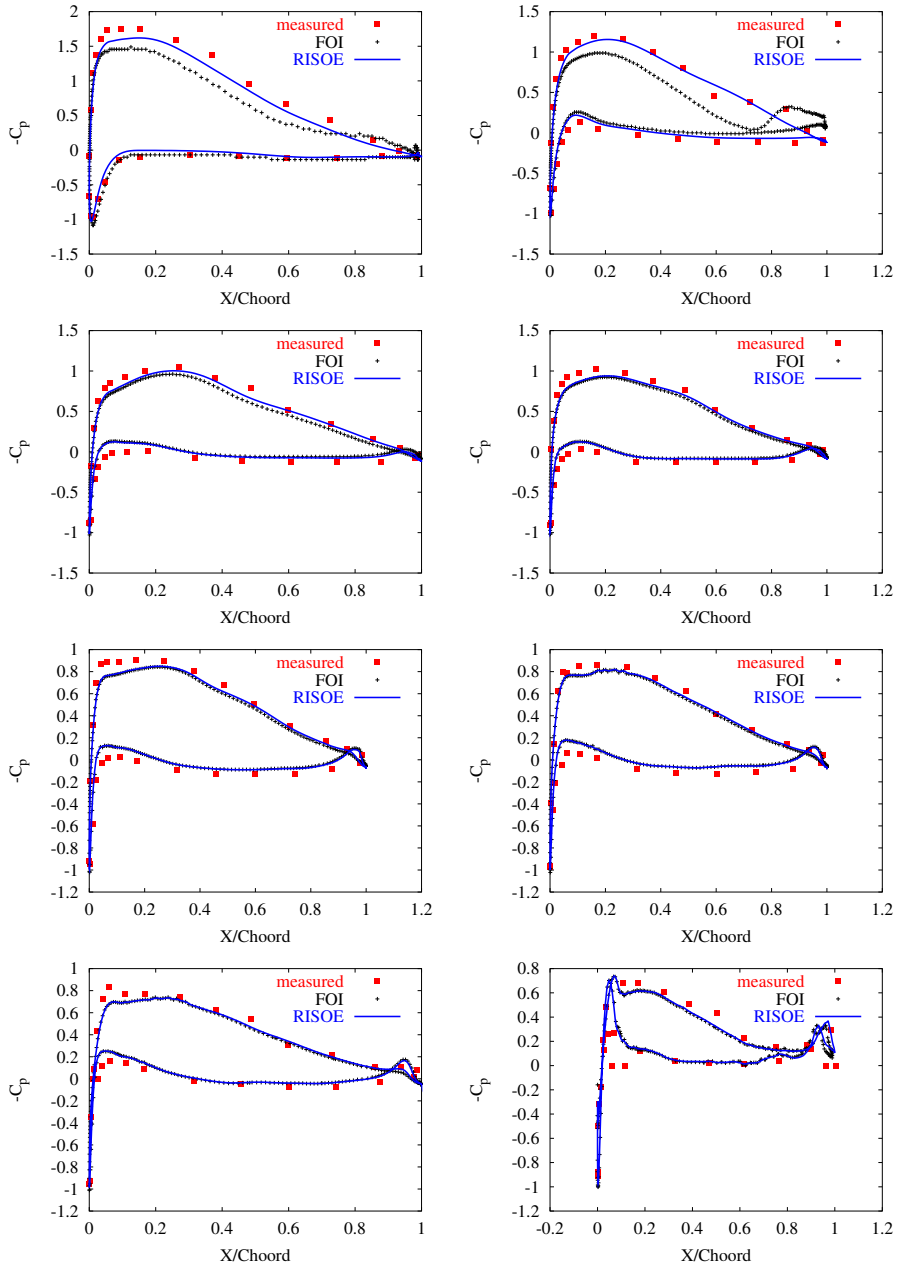

Figure 12. Comparison of computed and measured pressure for the free configuration of CASE 16 using the blockage corrected wind speed. The figure shows from top left to bottom right the spanwise sections [0.30, 0.55, 0.75, 0.85, 0.925, 0.95, 0.975, 0.99]

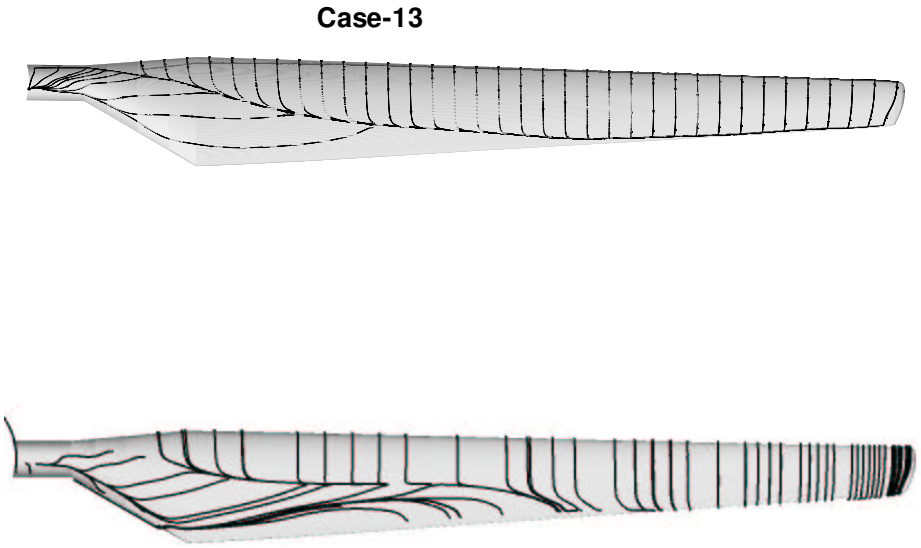

Figure 13. The limiting streamlines on the suction side of the blade for CASE 13 from the RISOE, top, and FOI computations, bottom.

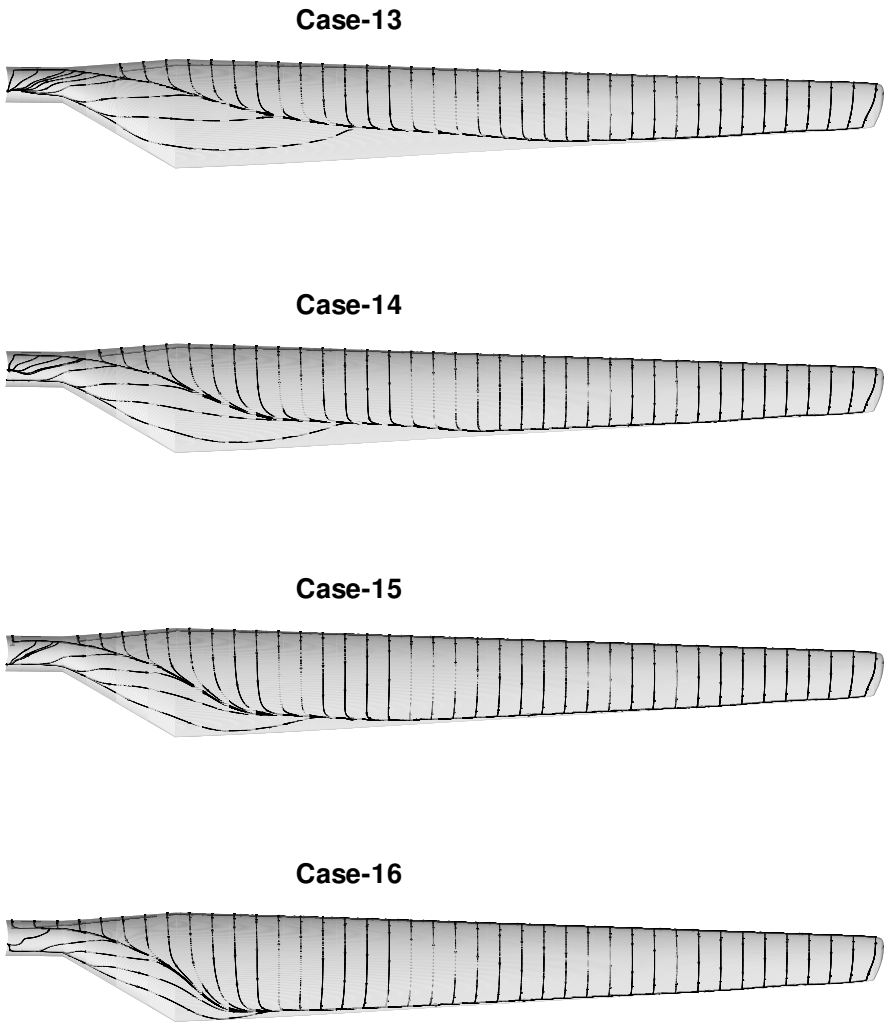

Figure 14. The limiting streamlines on the suction side of the blade derived from the RISOE computations. The figure show CASE 13 to 16 from top to bottom.

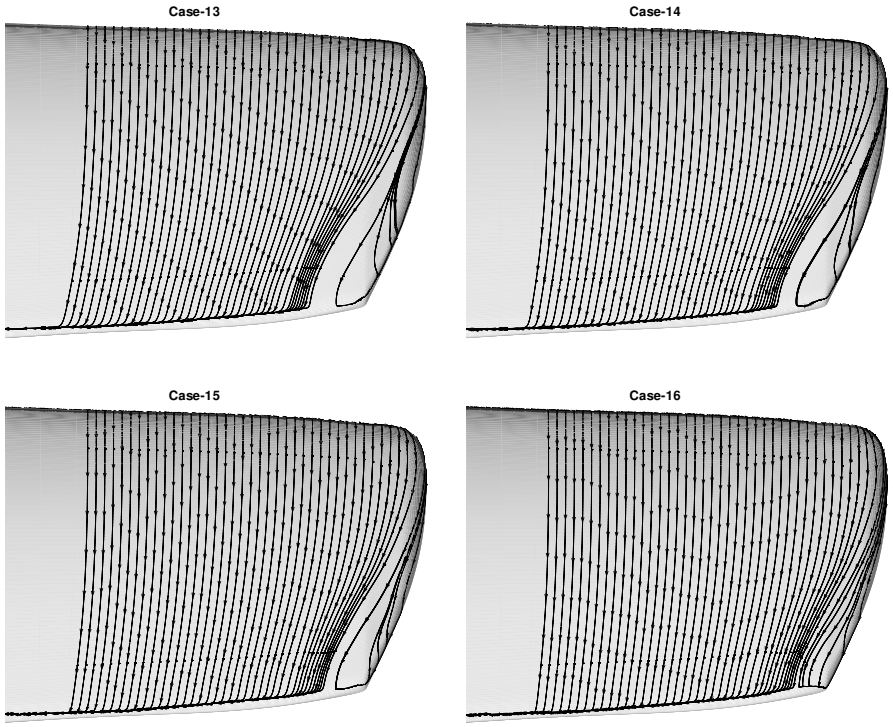

Figure 15. The limiting streamlines on the suction side of the tip part of the blade derived from the RISOE computations. The figure shows CASE 13 to 16 from top left to bottom right.

7 Results LM8.2

Having validated that state of the art CFD codes are capable of predicting quite accurately the airflow around a blade tip, an investigation of blade tips was initiated. Three series of test cases were taken from an experimental study [7]. Here a 95 kW Tellus wind turbine equipped with LM8.2 blades were studied using five different blade tips. In the present study we will focus on only three of these, namely the STANDARD tip, the TAPER tip and the SWEPT tip, see Figure 16. In the present comparison four wind speeds, 7, 10, 12, and 15 [m/s] are investigated. For all cases the rotational speed is 47.9 RPM, the air density is 1.225 kg/m^3, and the viscosity is 1.78791×10^{-5} $kg \times m^2/s$, the tip pitch angle is 1.8 degrees. Due to the additional computational requirements of rotors not aligned with the flow, the five degrees rotor tilt is neglected in the present computations. Three partners were involved in the study, namely NTUA, DLR and DTU. First the computations of the three partners are compared, and where available, also with measurements. Following the comparison of the computations a discussion of the different characteristics of the blade tips are given.

From the experimental data it is known that except for one of the tips, the TAPER tip, the influence of the tip geometry on overall power production characteristics of the turbine is very weak in the low wind speed region. The TAPER tip showed an increased power production over the hole range of wind speeds, but in the conclusion of the measuring report it is stated that this needs further verification [7]. For the remaining tips, a small increase in power production is observed in the measurements near max power, a phenomenon not reproduced by the CFD computations. As it is well known that CFD codes are not very accurate for highly separated flow, it is not surprising that they cannot capture the correct behaviour in this range of wind speeds. Comparing the three series of computations all three codes show very good agreement until 12 m/s, see Figure 17. For higher wind speeds, the DTU results overpredicts the produced power in good agreement with the normal observation using the $k-\omega$ SST turbulence model. The DLR results underpredicts the power production, and this may be connected to the use of the Spalart-Allmaras turbulence model in the TAU code of DLR known to predict separation earlier than the $k-\omega$ model. The computations of NTUA follow the power curve quite well. Studying the details of the flow, as will be done later on, indicate that errors connected to the boundary condition on the inboard part of the rotor and the location of the inboard boundary accidentally cancels out producing the correct results.

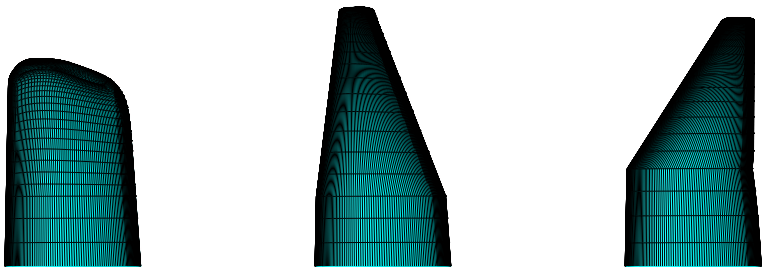

Figure 16. The three investigated blade tips, the STANDARD (left), the TAPER (middle) and the SWEPT tip (right). The leading edge of the tips are pointing to the left.

Having seen that until 12 m/s, where separation become important, a good

agreement is observed for all partners results, we will have a brief look at the tangential distributions of driving force F_x and the normal force F_z. For three lowest wind speeds 7, 10 and 12 in the STANDARD rotor case good agreements is observed especially for the driving force, see Fig. 18. For the highest wind speed, 15 m/s, the driving force shows that the lowering of the power production predicted by the DLR computations are originating from a stalled region near the blade tip, see Figure 18. For the SWEPT tip, again a good agreement is found between the DLR and DTU results for the lowest three wind speeds, while some peculiar behaviour is observed for the NTUA results, see Fig. 19. Starting with the driving force F_x it is observed that a good agreement is observed with the results from the DTU and DLR results for the last meter near the blade tip, while the force keeps increasing when approaching the root of the blade. This behaviour is not what would be expected, and an erroneous boundary conditions at the root section may be the reason. For the 10 and 12 m/s cases, the normal force computed by NTUA shows fair agreement with the other computations only for the outermost few meter of the blade span, see Figure 19. For the TAPER computations, where only DTU and NTUA have performed computations, similar behaviour is observed in the NTUA predictions, see Fig. 20. Again, the driving force is increasing all the way to the inboard boundary in the NTUA computations, whereas the DTU results shows the expected behaviour. As mentioned earlier, looking at the difference between the area under the DLR/DTU curves and the NTUA curve for the driving force on the SWEPT blade, and the area under the DLR/DTU curves on the inboard part of the rotor not included in the NTUA computations, it seems that these areas nearly cancel. This might be the explanation why the NTUA computations still predicts the correct power, even though the force distributions are unphysical near the inboard boundary.

Comparing the DLR and DTU C_p results for the STANDARD case, a very good agreement is observed between the two series of computations, see Figure 21-24. For the three lowest wind speeds, 7, 10 and 12 m/s, the agreement is excellent except for the innermost radial station where the low Mach number introduces wiggles in the compressible solution of DLR. Near the stagnation points deviation are also observed, which again may be connected to the low Mach number in this region. For the remaining stations the agreement is excellent, and the slightly confusing lines at r=9.2 and r=9.4 in the DTU results are a post processing problem related to the ordering of the points in the result files. For the highest wind speed, 15 m/s, the agreement is not as good, and this is connected to the DLR code predicting leading edge flow separation, while the DTU model predicts the flow to be still attached. As mentioned previously, other computations has shown that the Spalart-Allmaras model has a greater tendency to predict flow separation than the $k-\omega$ SST model used by DTU.

For the SWEPT blade, the comparison of the DTU and DLR results are nearly identical to what has just been reported for the STANDARD case, see Fig. 25-28. Finally, comparing the NTUA results with the results of the other partners, the solution is again seen to deviate predicting a excessive suction near the leading edge especially for the four outermost sections. Based on the validation on the STORK rotor between the FOI EDGE code, and the RISOE/DTU code EllipSys3D and the good agreement between the DLR TAU code, and the RISOE/DTU code EllipSys3D one may conclude that it is the NTUA results that are incorrect.

Having verified that at least the DLR and DTU prediction for the lowest three wind speeds show good agreement, and based on the validation in connection with the STORK rotor, it is believed that the tip predictions can be trusted for the lowest three wind speeds. For the highest wind speed, 15 m/s, the well-known problem of Navier-Stokes predictions of separated flow will influence the accuracy of the predictions.

Having the detailed CFD predictions of the tip flows, it is possible to visualize the limiting streamlines on the blade tips. Here the skin friction on the tip surface is used to compute streamlines on the blade surface, creating pictures similar to oil flow visualizations. In Figure 33 the limiting streamline patterns are compared for the three tips at the four selected wind speeds examined. The wind speed is increased from the 7 m/s at the top row of the figure to 15 m/s at the bottom row of the figure. At the lowest two wind speeds no sign of separation on any of the blade tips can be observed, except for the tip vortex right at the tip of the blades. With the increase of wind speed the part of the surface area influenced by the tip vortex is enlarged. For the 12 m/s wind speed the SWEPT tip shown in the middle row of the figure features a large vortex structure, while both the STANDARD and the TAPER tip are still topologically equal to the 7 m/s cases. For the 15 m/s cases, both the SWEPT and the TAPER tip exhibits vortical structures on the blade tip, while the STANDARD tip still resembles the low speed flow topology.

Based on the CFD solutions, boundary layer parameters can be extracted and used in empirical noise models. As this has not been the scope of this work, this path has not been pursued. Additionally, airfoil data extracted from the CFD solution can be used to predict the aerodynamic damping properties of the blades to estimate which tip shape is most optimal in connection with damping of structural vibrations in the rotor blades.

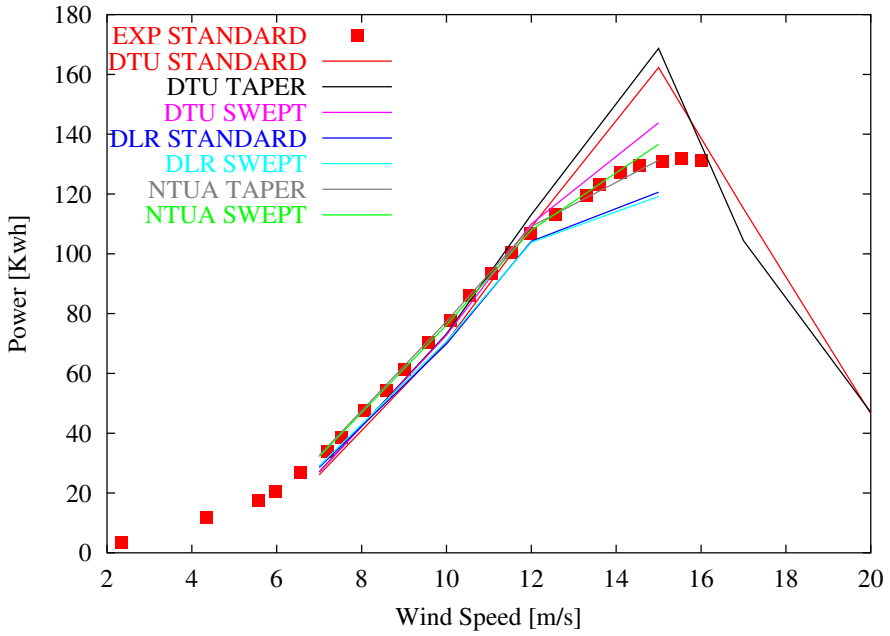

Figure 17. Comparison of the mechanical power predicted by the three series of computations and the measured power for the STANDARD blade.

8 Conclusion LM8.2 blades

In the present work three Navier-Stokes codes has been compared with available measurements from an experiment on the LM8.2 rotor blade. Two of these codes, the DLR and DTU/RISOE code show good agreement for wind speeds up to 12 m/s. As the comparison of the DTU/RISOE code and the FOI code with

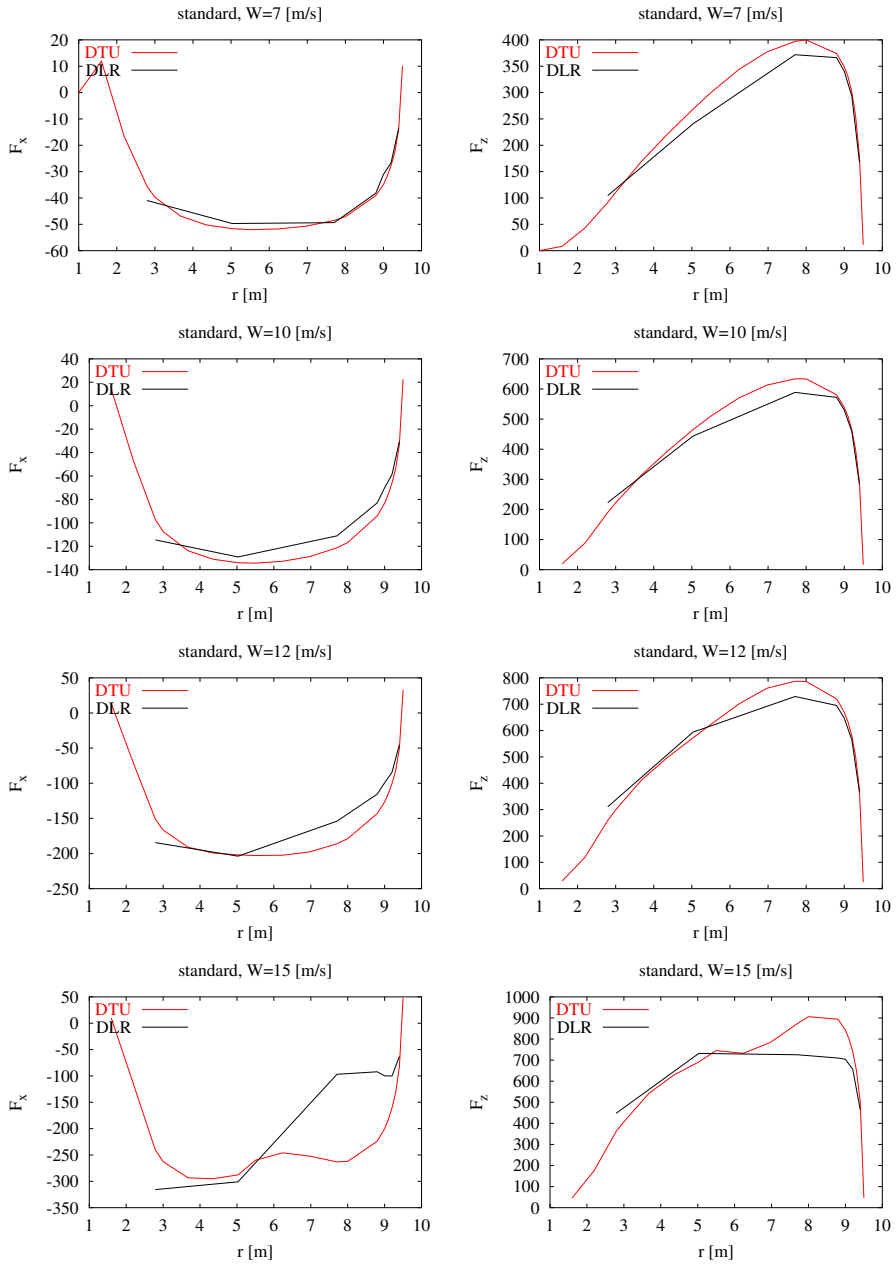

Figure 18. Spanwise distributions of the tangential (driving) and axial (thrust) force for the STANDARD rotor.

experiments for the STORK WPX 5 rotor, has shown good agreement, there is substantial evidence that CFD codes can be used for predicting tip flows, and provide details that cannot be obtained by simpler aerodynamic models as lifting line or Blade Element Momentum methods. Unfortunately, the NTUA predictions differs significantly from the remaining results, and problems with the inner boundary conditions or the fact that the NTUA predictions are not computed on the common meshes, may be the explanation of these differences. Additionally it has been shown, that the detailed pressure distributions and limiting streamline plots can be used to obtain insight into the actual flow physics on blade tips.

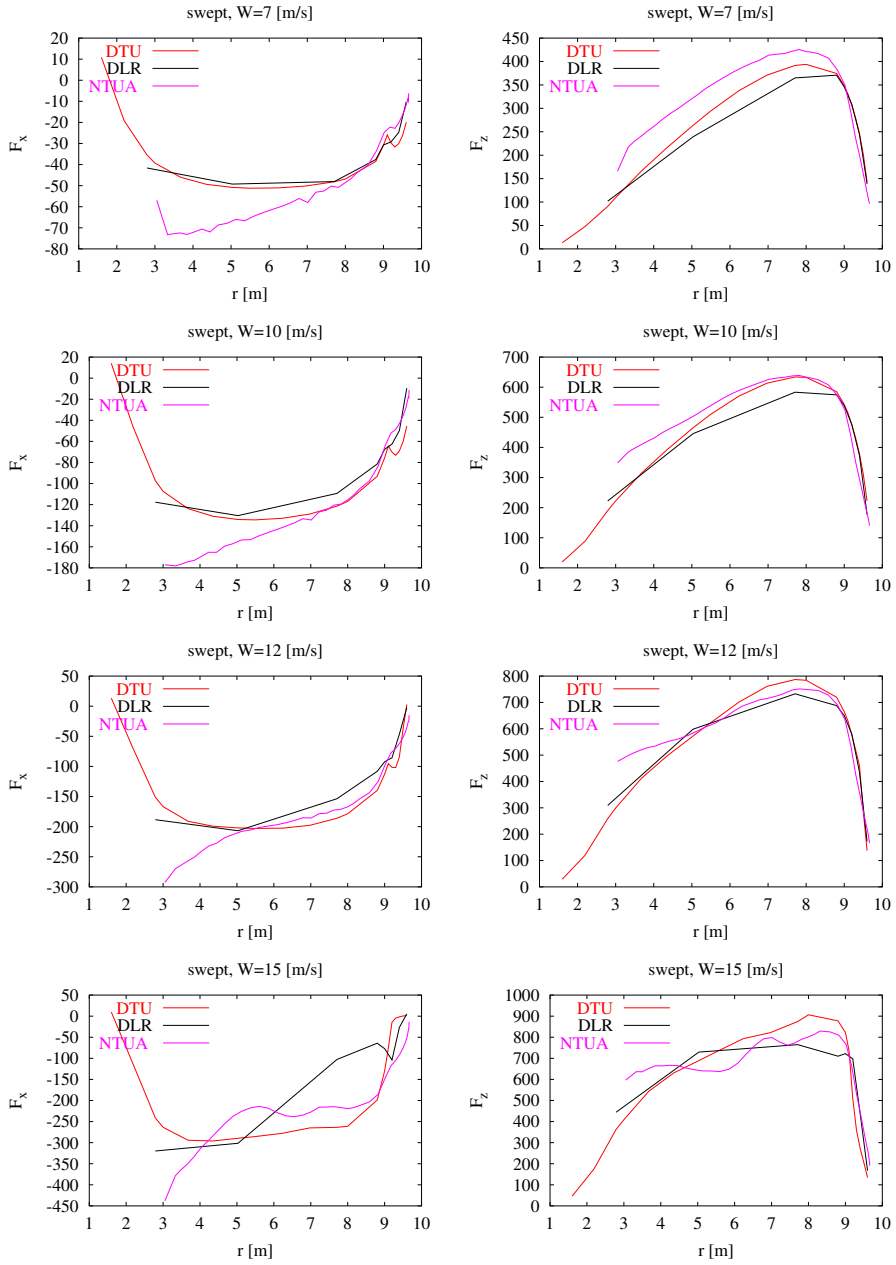

Figure 19. Spanwise distributions of the tangential (driving) and axial (thrust) force for the SWEPT rotor.

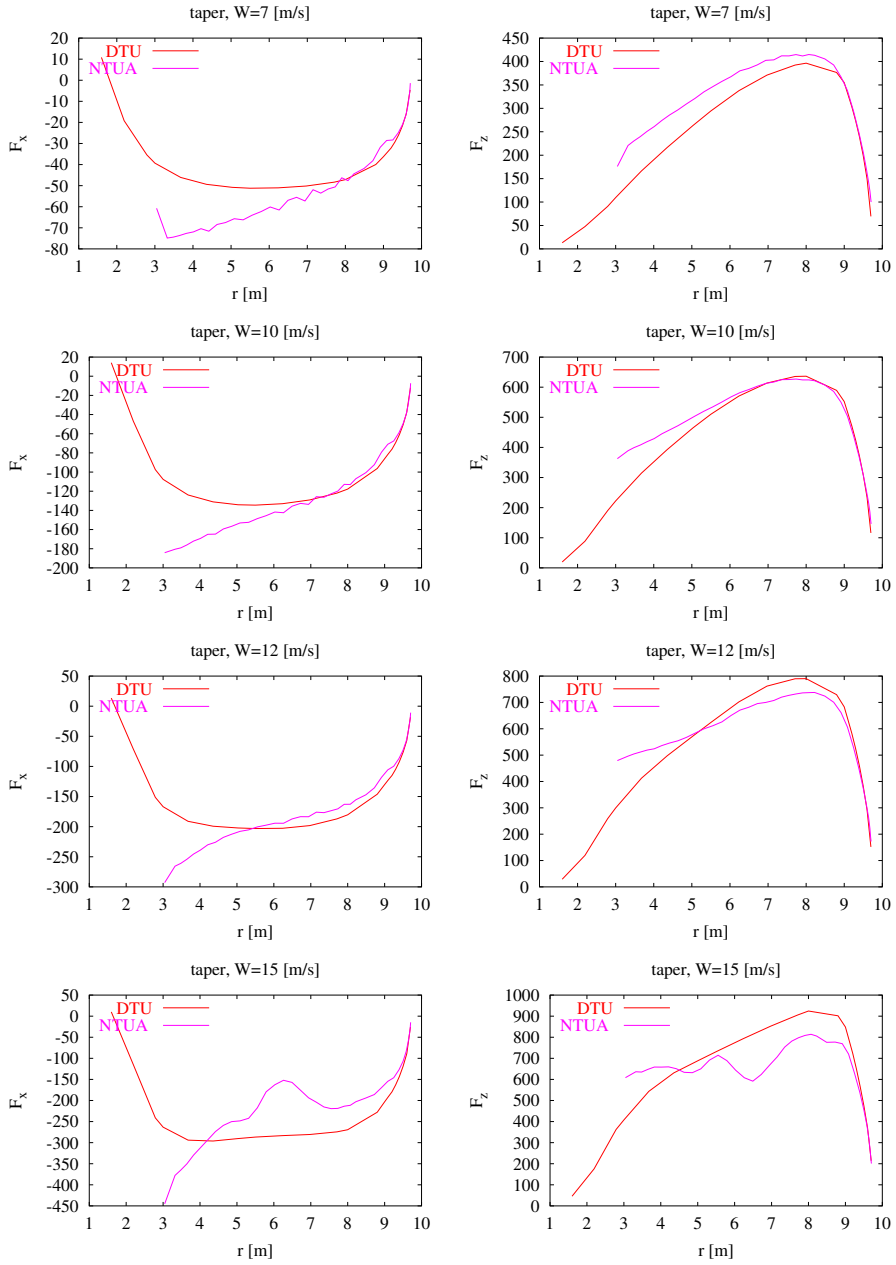

Figure 20. Spanwise distributions of the tangential (driving) and axial (thrust) force for the TAPER rotor.

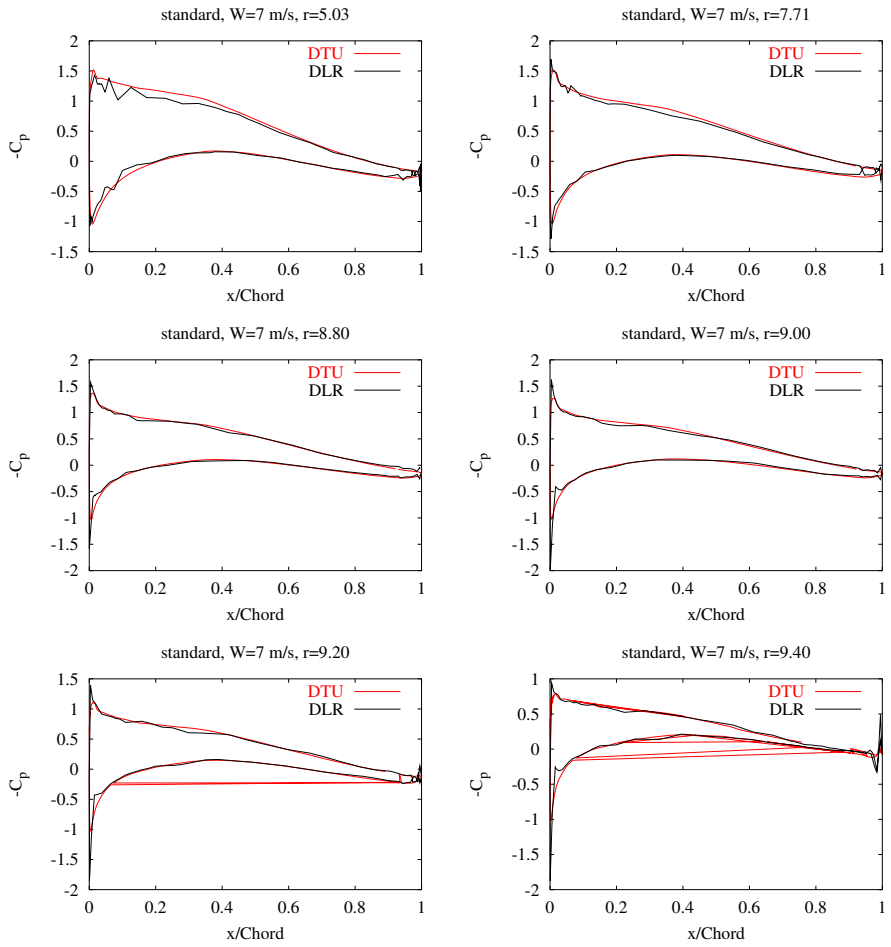

Figure 21. Pressure distributions at six spanwise positions along the STANDARD rotor at 7 m/s.

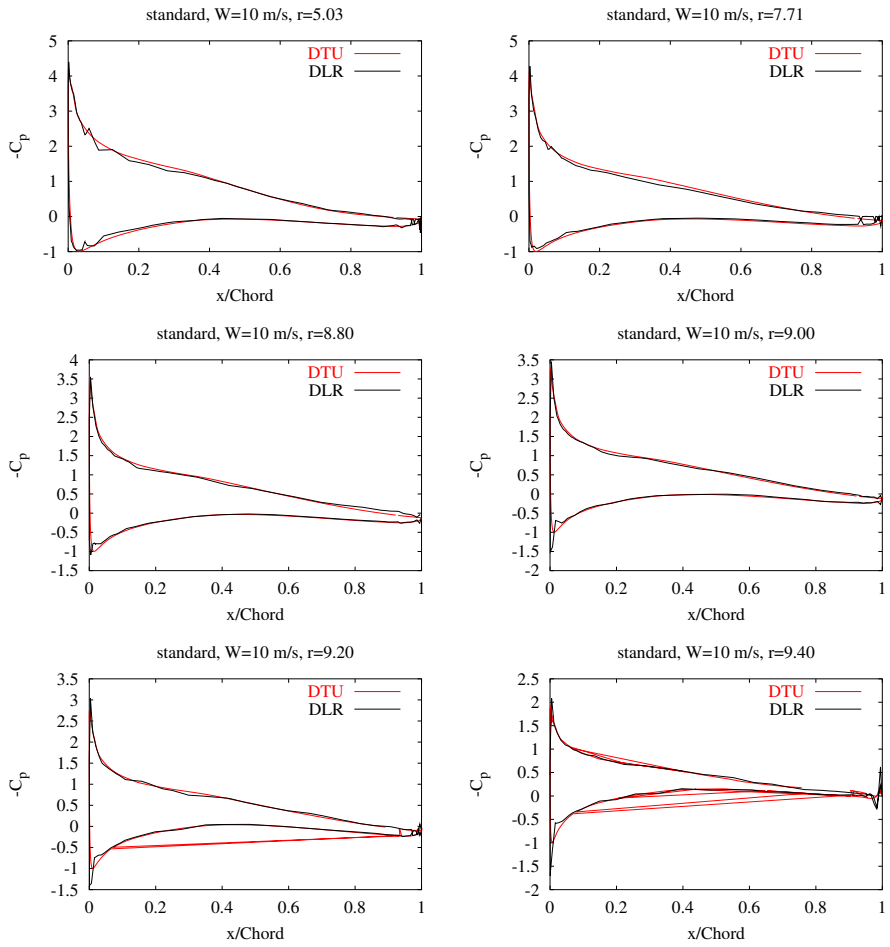

Figure 22. Pressure distributions at six spanwise positions along the STANDARD rotor at 10 m/s.

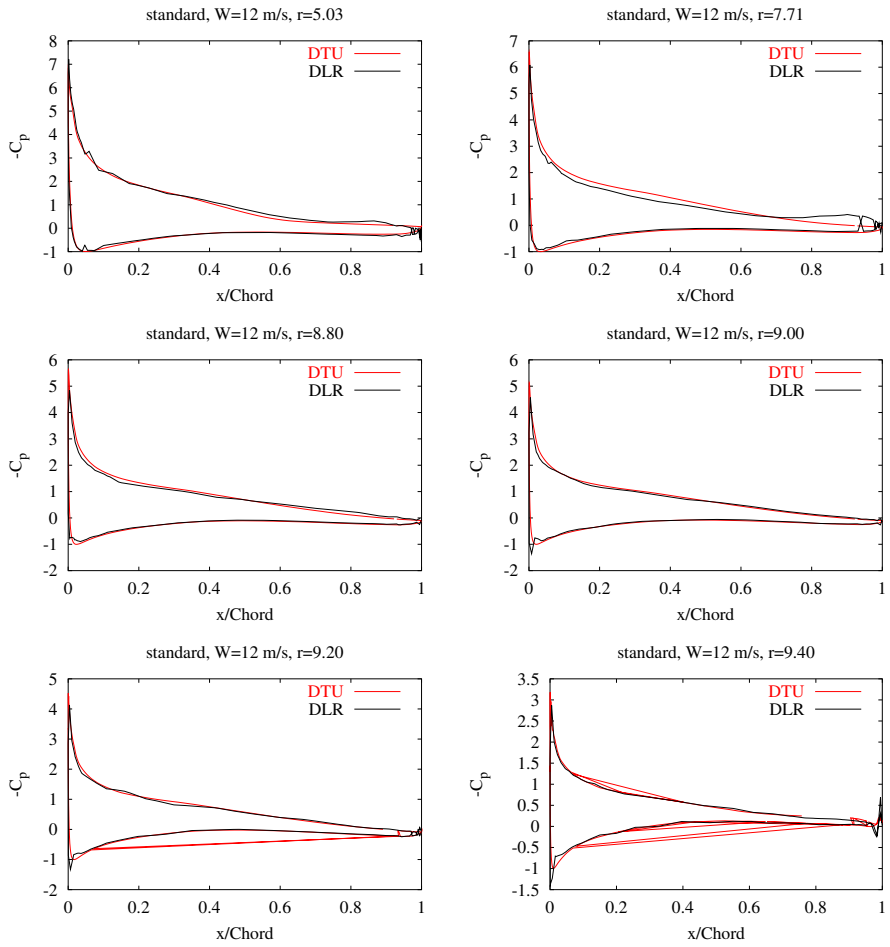

Figure 23. Pressure distributions at six spanwise positions along the STANDARD rotor at 12 m/s.

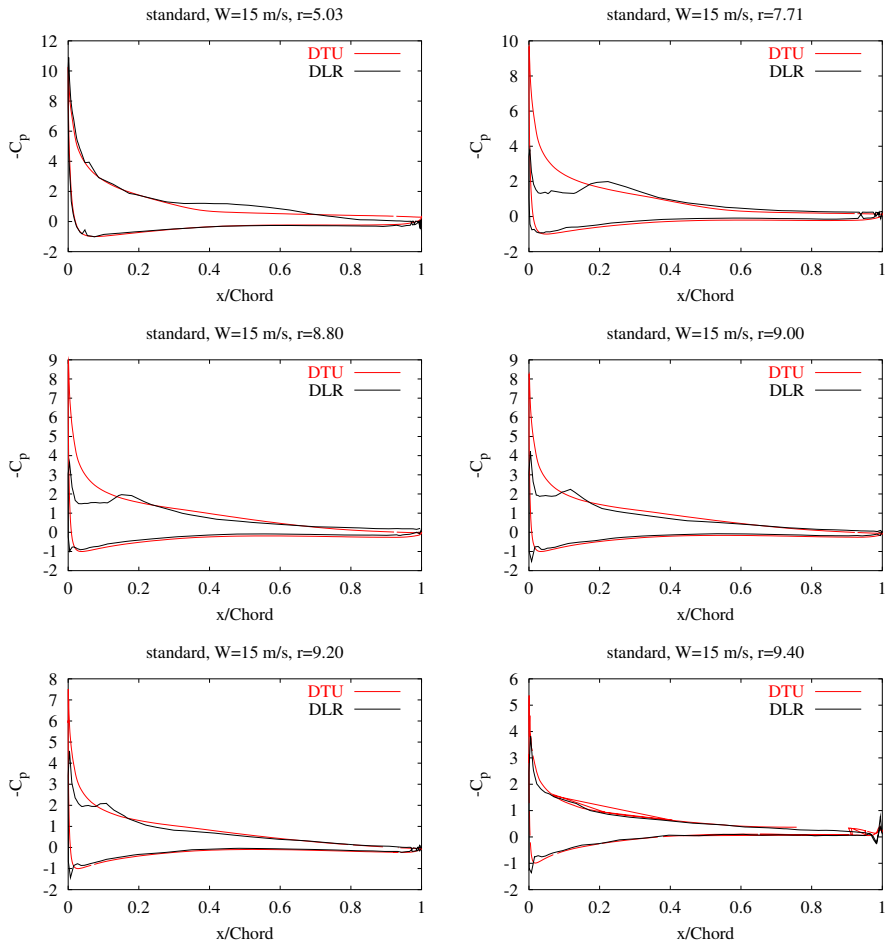

Figure 24. Pressure distributions at six spanwise positions along the STANDARD rotor at 15 m/s.

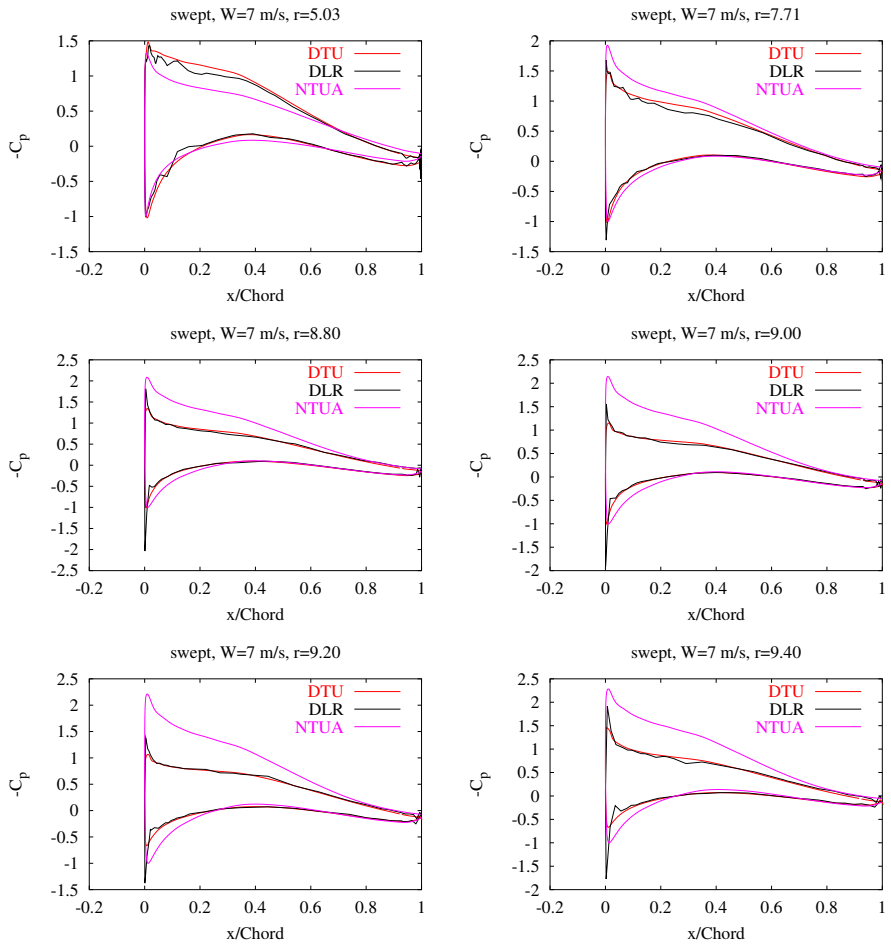

Figure 25. Pressure distributions at six spanwise positions along the SWEPT rotor at 7 m/s.

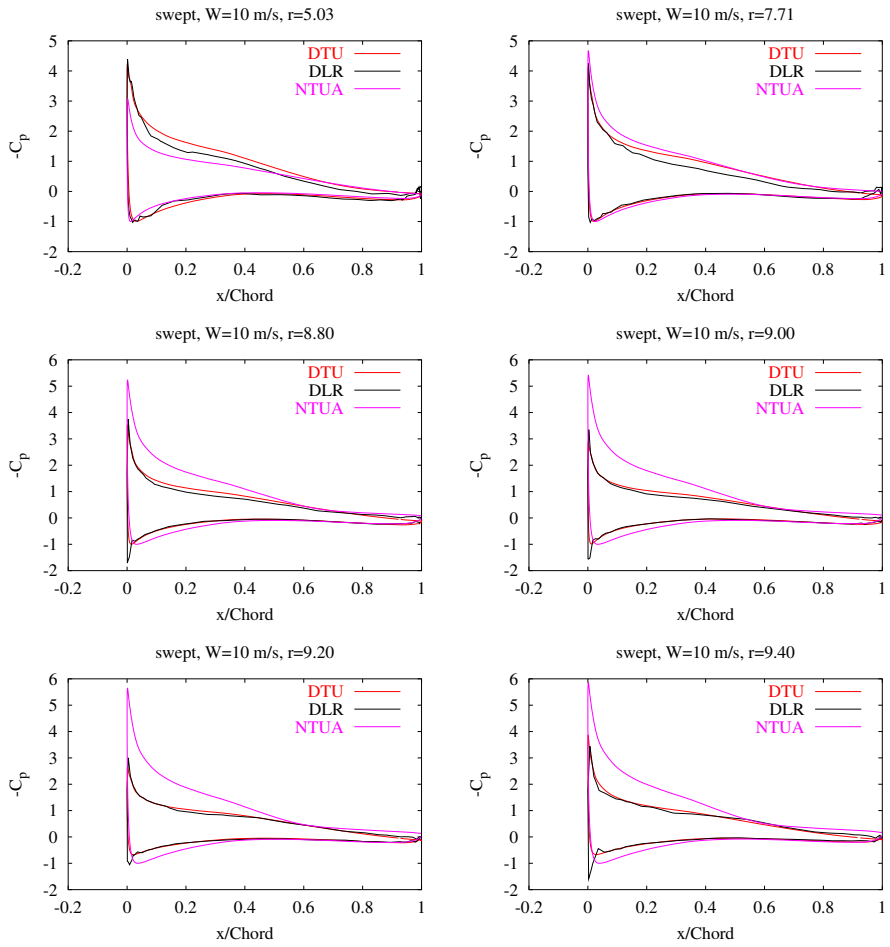

Figure 26. Pressure distributions at six spanwise positions along the SWEPT rotor at 10 m/s.

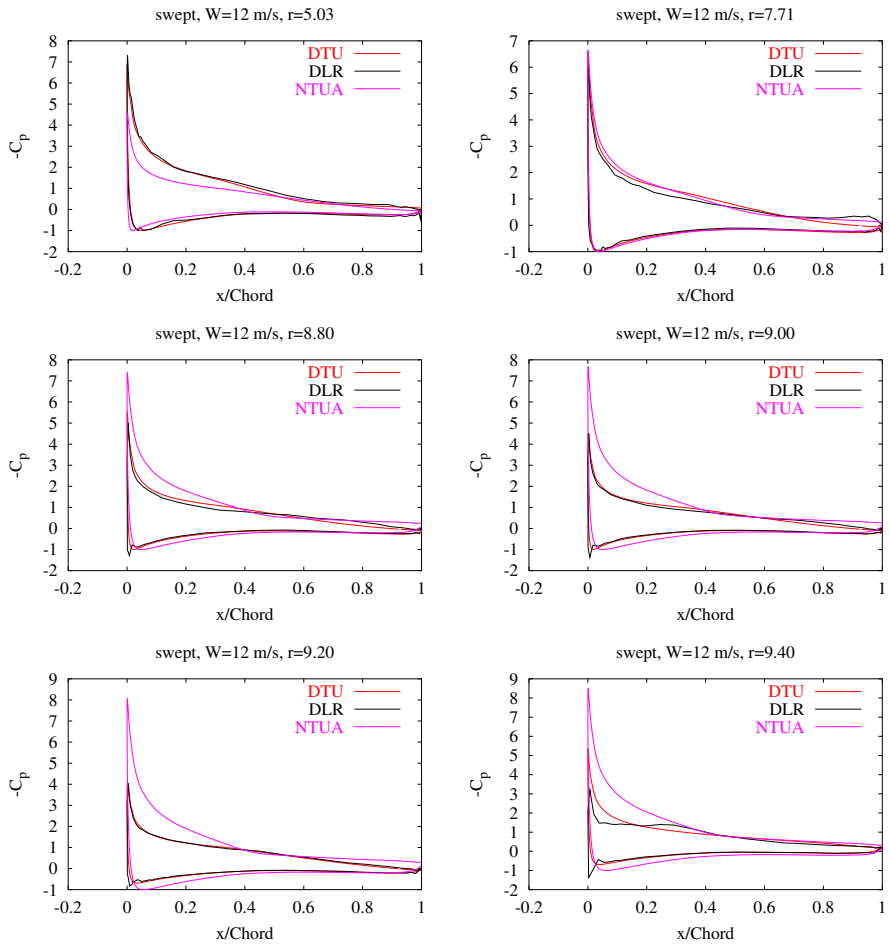

Figure 27. Pressure distributions at six spanwise positions along the SWEPT rotor at 12 m/s.

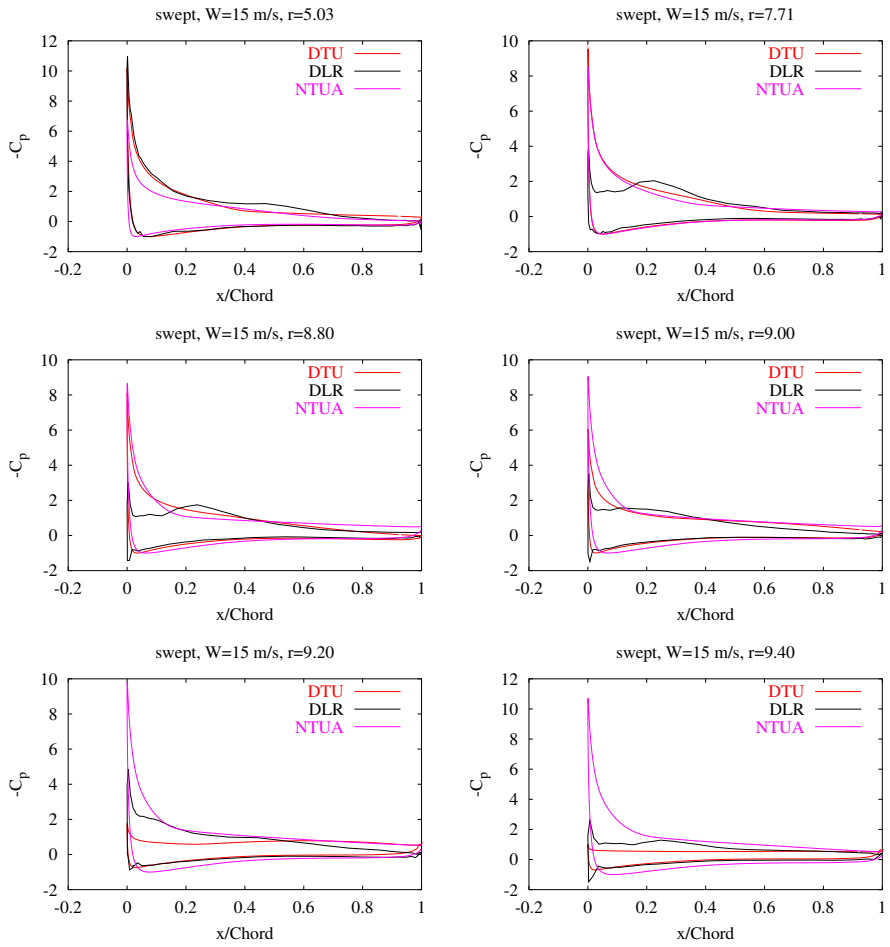

Figure 28. Pressure distributions at six spanwise positions along the SWEPT rotor at 15 m/s.

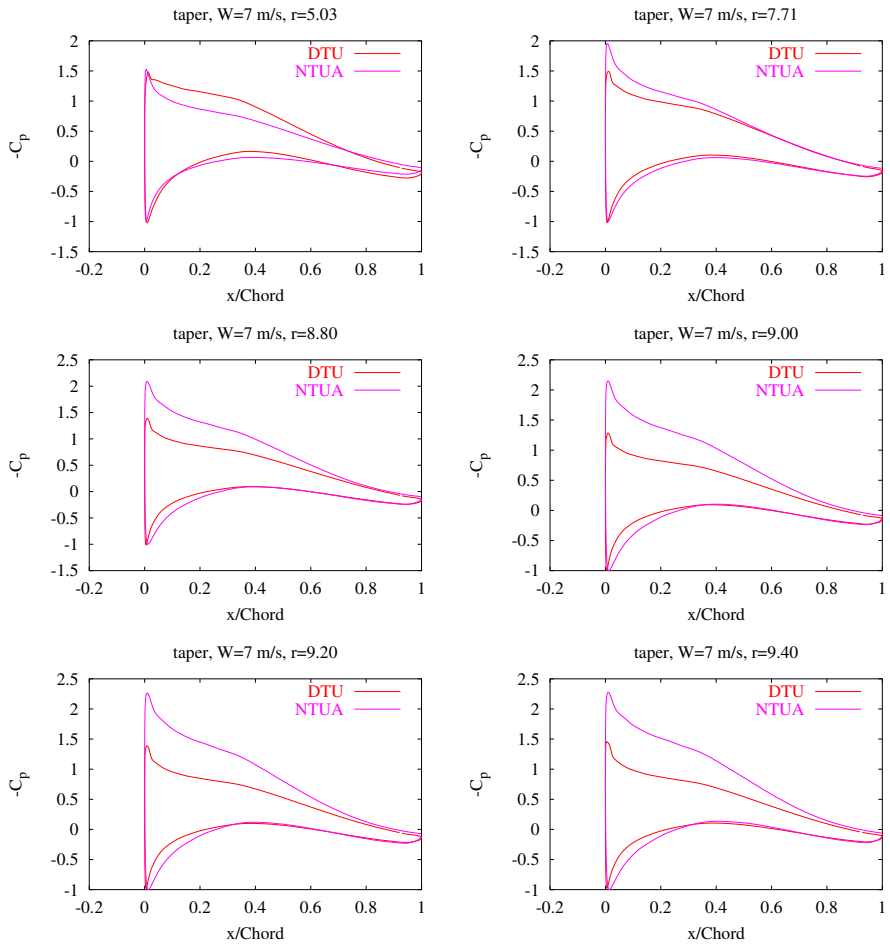

Figure 29. Pressure distributions at six spanwise positions along the TAPER rotor at 7 m/s.

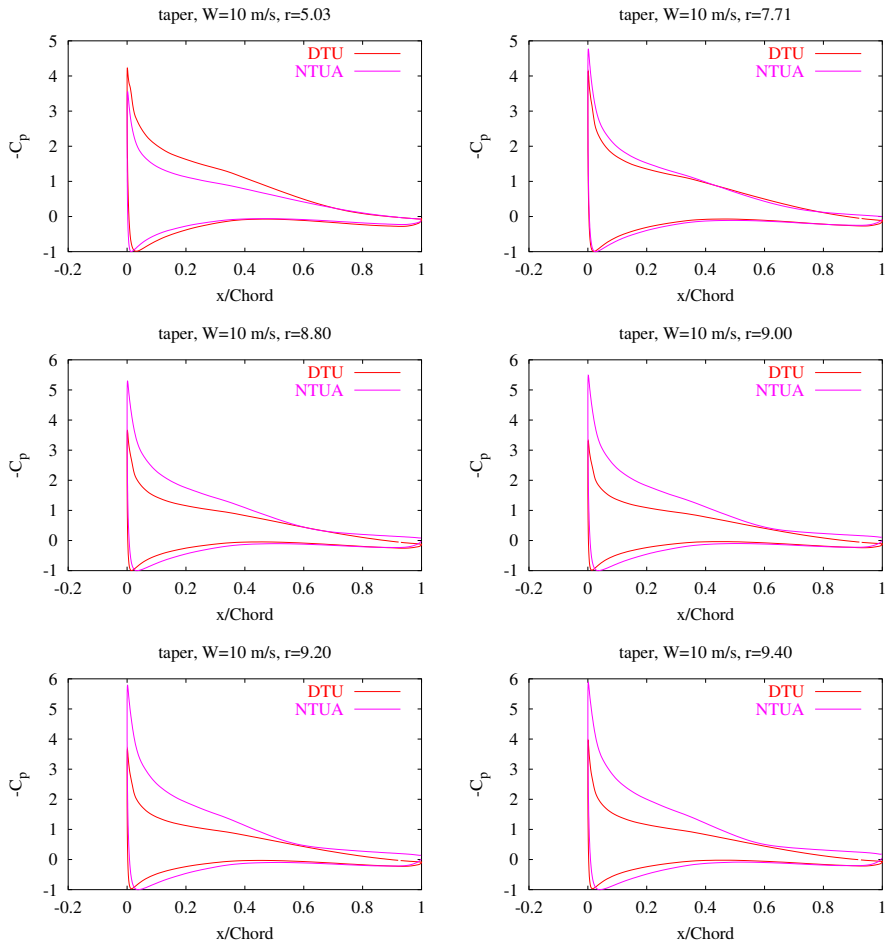

Figure 30. Pressure distributions at six spanwise positions along the TAPER rotor at 10 m/s.

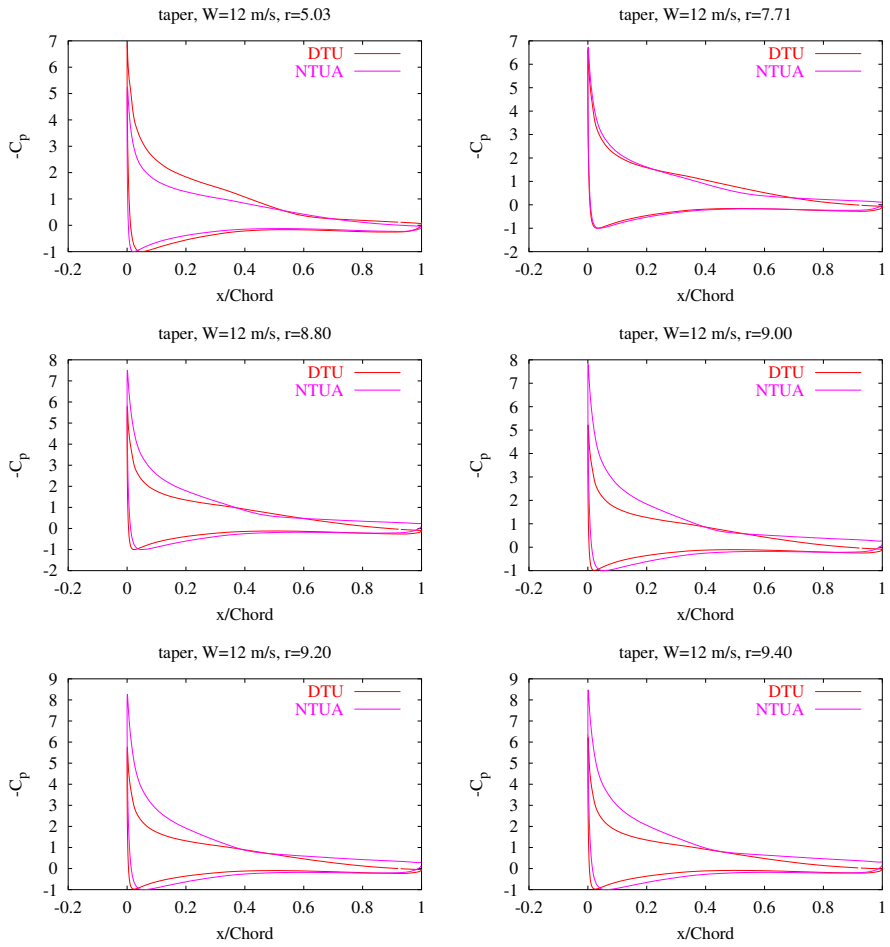

Figure 31. Pressure distributions at six spanwise positions along the TAPER rotor at 12 m/s.

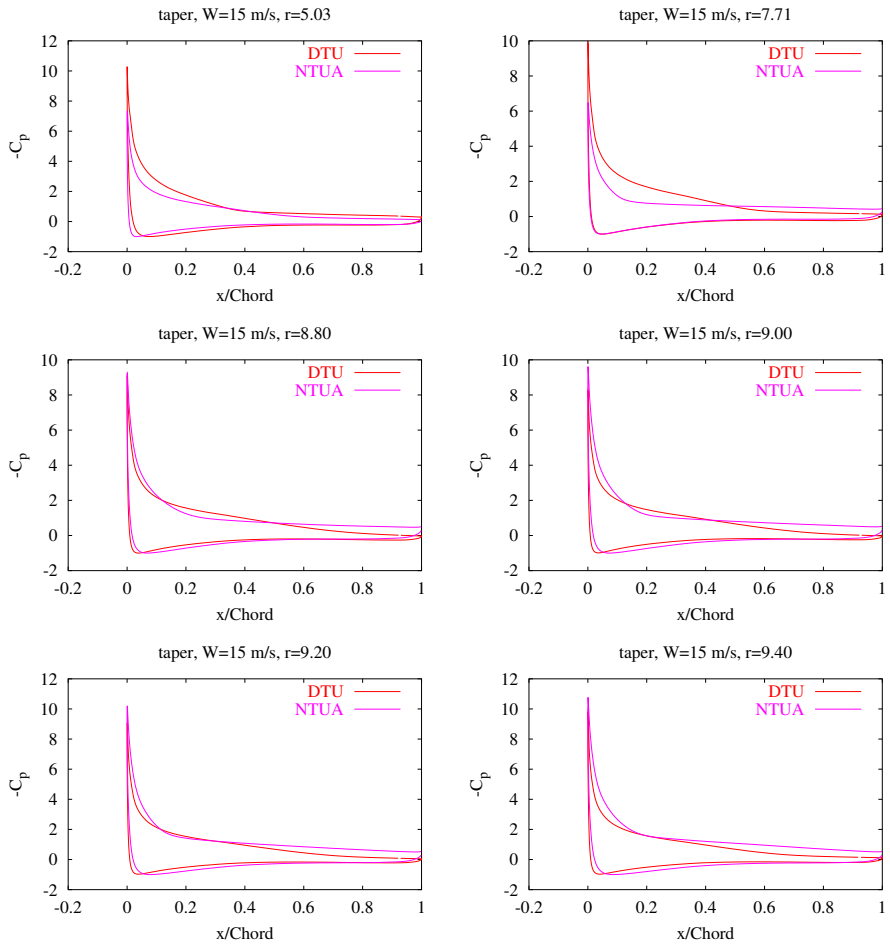

Figure 32. Pressure distributions at six spanwise positions along the TAPER rotor at 15 m/s.

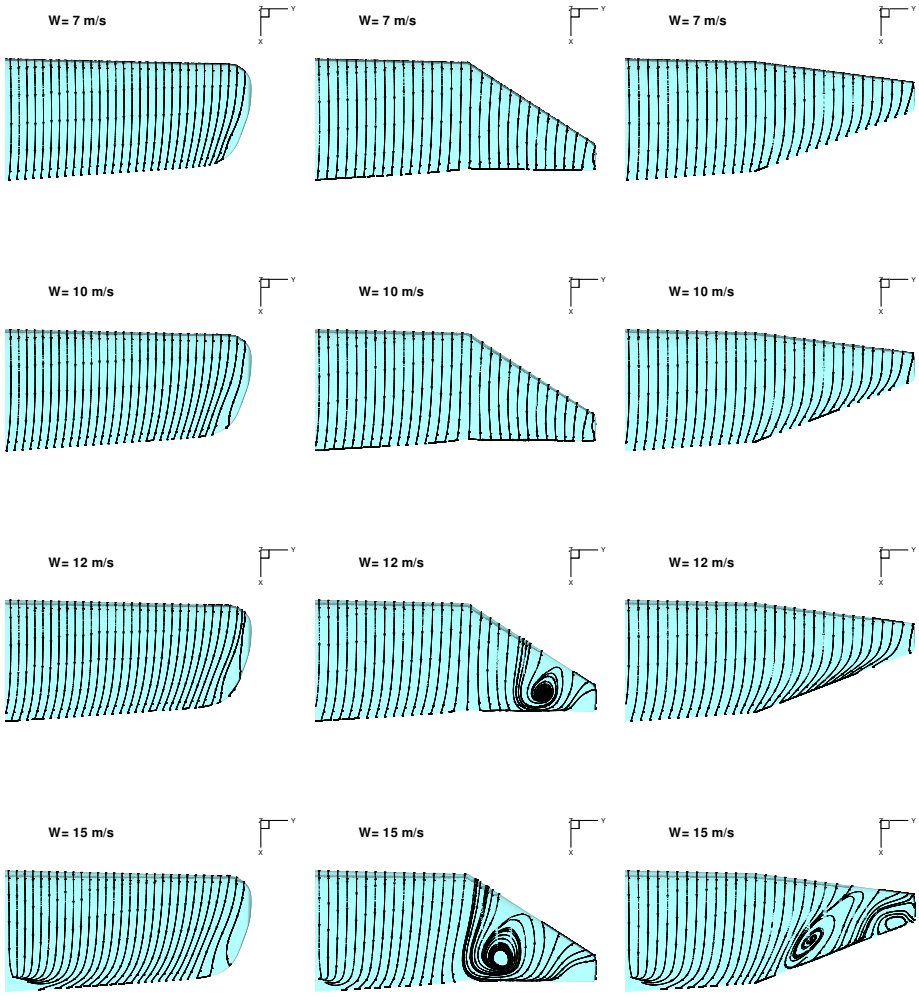

Figure 33. Limiting streamlines on the suction side of the three different blade tips for six wind speeds each.

9 Conclusion

The present tip shape study has shown that modern CFD codes predict consistent results, where three of the four applied solvers give very similar results. The problems observed with the fourth solver, may either be connected to an erroneous boundary condition at the inboard boundary, or the fact that an alternative mesh that may have inferior quality with respect to resolution of the flow and the location of the outer boundaries. Besides predicting similar results, the three of the solvers also show good agreement with the available measurements. The agreement is best for high tip speed ratios where flow is far from separation, and on the outboard part of the blade. With respect to tip studies, the area of interest is located exactly at the outboard stations where the angles of attack are low.

The study has shown that the pressure distributions on the blade tip can be quite accurately predicted. From previous studies it has been shown that airfoil data can be extracted for use in Blade Element Momentum methods to study the aeroelastic behaviour of wind turbine rotors. Alternatively, the CFD methods can be directly coupled to elastic models to study aeroelastic behaviour of tip shapes.

Besides, the direct loading on the turbine blades the CFD solutions can also be used to obtain qualitative information about the flow pattern on the blade surface, in the form of limiting streamlines. Using the detailed normal velocity distributions boundary layer heights at the trailing edge can be determined and used in connection with noise modelling.

The overall conclusion of this tip study is that CFD is a powerful tool if advanced tip shapes has to be evaluated in connection with a new blade design.

10 Acknowledgement

The work was carried out under a contract with the EC, ENK6-CT-2001-00503, KNOW-BLADE. Computations by RISOE were made possible by the use of the IBM RS6000 SP at the Risø central computing facility and the Danish Centre for Scientific Computing Linux cluster Yggdrasill facility in Lyngby, Denmark.

References

[1] Madrane A., Raichle A., and Stuermer A. Parallel Implementation of a Dynamic Unstructured Chimera Method in the Finite Volume TAU-Code. pages 524–534, Ottawa, Ontario, Canada, 2004.

[2] Madrane A., Heinrich R., and Gerhold T. Implementation of the Chimera Method in the Unstructred Hybrid DLR Finite Volume TAU-code. Ft. Walton Beach, FL., USA, 2002.

[3] A. Bjorck, G. Ronsten, and B. Montgomerie. Aerodynamic Section Characteristics of a Rotating and Non-rotating 2.375 m Wind Turbine Blade. FFA TN 1995-03, FFA, Bromma, Sweden, 1995.

[4] Wilcox D. C. A Half Century Historical Review of the K-ω Model. AIAA-91-0615, 1991.

[5] Simms D., Schreck S., Hand M., and Fingersh L.J. NREL Unstead Aeorydnamics Experiment in the NASA-Ames Wind tunnel: A Comparison of Predictions to Measurements. NREL/TP -500-29494, Nat. Ren. Energy Lab., Golden, CO, 2001.

[6] Rönsten G. Geometry and Installation in Wind Tunnels of a STORK 5.0 WPX Wind Turbine Blade Equipped with Pressure Taps. Technical Report FFAP-A 1006, 1994.

[7] Antoniou I., Madsen H.A., and Paulsen U.S. Influence of the tip Shape on the Aerodynamic Behavior of A Wind turbine Rotor. Risø-I- 910-(EN), Risø National Laboratory, Roskilde, Denmark, December 1995.

[8] Issa R. I. Solution of the Implicitly Discretised Fluid Flow Equations by Operator-Splitting. *J. Computational Phys.*, 62:40–65, 1985.

[9] Issa R. I., Gosman A. D., and Watkins A. P. The Computation of Compressible and Incompressible Recirculating Flows by a Non-iterative Implicit Scheme. *J. Computational Phys.*, 62:66–82, 1986.

[10] Michelsen J.A. Basis3D - a Platform for Development of Multiblock PDE Solvers. Technical Report AFM 92-05, Technical University of Denmark, 1992.

[11] Michelsen J.A. Block structured Multigrid solution of 2D and 3D elliptic PDE's. Technical Report AFM 94-06, Technical University of Denmark, 1994.

[12] Michelsen J.A. General curvilinear transformation of the Navier-Stokes equations in a 3D polar rotating frame. Technical Report ET-AFM 98-01, Technical University of Denmark, 1998.

[13] Petersen J.M., Madsen H.A., Björck A., Enevoldsen P., Øye S., Ganander H., and Winkel aar D. Prediction of Dynamic Loads and Induced Vibrations In Stall. Risø-I- 1045-(EN), Risø National Laboratory, Roskilde, Denmark, May 1998.

[14] Khosla P. K. and Rubin S. G. A diagonally dominant second-order accurate implicit scheme. *Computers Fluids*, 2:207–209, 1974.

[15] Braun K.A., Arnold H., Gordner A., Hailer F., Huurdeman B., and Müller M. Some Blade Tip Modifications and their Influence on Aeroacoustics. In *Proc. European Wind Energy Conference*, pages 90–94, Göteborg, Sweeden, May 20-24 1996.

[16] Hand M., Simms D., Fingersh L.J., Jager D., and Larwood S. Cotrell J., Schreck S. Unsteady Aeorydnamics Experiment Phases VI: Wind tunnel Test Configurations and Available Data Campaigns. NREL/TP -500-29955, Nat. Ren. Energy Lab., Golden,CO, 2001.

[17] Kroll N., Rossow C.-C., Becker K., and Thiele F. The megaflow project. *Aerospace Science and Technology*, 4:223–237, 2000.

[18] Sørensen N. N. General Purpose Flow Solver Applied to Flow over Hills. Risø-R- 827-(EN), Risø National Laboratory, Roskilde, Denmark, June 1995.

[19] Sørensen N.N. and Michelsen J.A. Aerodynamic Predictions for the Unsteady Aerodynamics Experiment Phase-II Rotor at the National Renewable Energy Laboratory. AIAA Paper 2000-0037, 2000.

[20] Eliason P. EDGE, a Navier-Stokes solver for unstructured grids. Technical Report FOI-R–0298–SE, 2002.

[21] Menter F. R. Zonal Two Equation k-ω Turbulence Models for Aerodynamic Flows. AIAA-paper-932906, 1993.

[22] Spalart P. R. and Allmaras S. R. A One-Equation Turbulence Model for Aerodynamic Flows. AIAA-paper-92-0439, 1992.

[23] Rönsten G. Aerodynamic Section Characteristics of a Rotating and Non-rotating 2.375 m Wind Turbine Blade. FFA TN 1995-03, FLygtekniska Forsoksanstalten, Bromma Sweeden, 1995.

[24] Rönsten G. and Dahlberg J.Å. and Meijer S. Static Pressure Measurements on A Rotating and a Non-Rotating 2.375 m Wind Turbine Blade - Comparison With 2D Calculations. In *Proc. European Wind Energy Conference*, pages 729–735, Glasgow, Scotland, July 10-13 1989.

[25] Wallin S. and Johansson A. A complete explicit Algebraic Reynolds Stress Model for Incompressible and Compressible Turbulent Flows. *JFM*, (403):89–132, 2000.

Bibliographic Data Sheet **Risø-R-1495(rev)(EN)**

Title and author(s)

KNOW-BLADE, Task-3.2 report, Tip Shape Study, revised version

N. N. Sørensen, J. Johansen, S. Conway, S. Voutsinas, M.O.L. Hansen, A. Stürmer

Abstract (Max. 2000 char.)

For modern rotor blades with their very large aspect ratio, the blade tip is a very limited part of the overall rotor, and as such of limited importance for the overall aerodynamics of the rotor. Even though they may not be very important for the overall power production, the tip noise can be very important for the acoustics of the rotor [15], and the blade tips can as well be important for the aerodynamic damping properties of the rotor blades [13]. Unfortunately, not many options exists for predicting the aerodynamic behavior of blade tips using computational methods. Experimentally it is difficult to perform detailed measurements in the form of pressure and velocity measurements in natural wind conditions on modern large scale turbines due to the inherent unsteadiness in the natural wind.
The present study describes the application of four different Navier-Stokes solvers to tip shape studies, and shows that these codes are well suited to study the flow around different tip shape geometries, and can predict the pressure distributions at the blade tip quite accurately.

ISBN

(Internet)

ISSN

ISBN 87-550-3429-2

Dept. or group

Risø National Laboratory
Wind Energy Department

Date

Jan 2005

Groups own reg. number(s)	Project/contract No.
1110033-00	ENK6-CT2001-00503

Pages	Tables	Illustrations	References
49	4	33	25

Descriptors INIS/EDB

AERODYNAMICS; AIRFOILS; COMPUTATIONAL FLUID DYNAMICS; FLOW MODELS; NAVIER-STOKES EQUATIONS; THREE-DIMENSIONAL CALCULATIONS; TURBINE BLADES; TURBULENT FLOW; WIND TURBINES